ACADEMIC PRESS

Available online at www.sciencedirect.com

SCIENCE DIRECT®

Journal of Computational Physics 187 (2003) 137–167

JOURNAL OF COMPUTATIONAL PHYSICS

www.elsevier.com/locate/jcp

Modeling uncertainty in flow simulations via generalized polynomial chaos

Dongbin Xiu, George Em Karniadakis *

Division of Applied Mathematics, Brown University, Providence, RI 02912, USA

Received 15 February 2001; received in revised form 10 October 2002; accepted 19 October 2002

Abstract

We present a new algorithm to model the input uncertainty and its propagation in incompressible flow simulations. The stochastic input is represented spectrally by employing orthogonal polynomial functionals from the Askey scheme as trial basis to represent the random space. A standard Galerkin projection is applied in the random dimension to obtain the equations in the weak form. The resulting system of deterministic equations is then solved with standard methods to obtain the solution for each random mode. This approach can be considered as a generalization of the original polynomial chaos expansion, first introduced by Wiener [Am. J. Math. 60 (1938) 897]. The original method employs the Hermite polynomials (one of the 13 members of the Askey scheme) as the basis in random space. The algorithm is applied to micro-channel flows with random wall boundary conditions, and to external flows with random freestream. Efficiency and convergence are studied by comparing with exact solutions as well as numerical solutions obtained by Monte Carlo simulations. It is shown that the generalized polynomial chaos method promises a substantial speed-up compared with the Monte Carlo method. The utilization of different type orthogonal polynomials from the Askey scheme also provides a more efficient way to represent general non-Gaussian processes compared with the original Wiener–Hermite expansions.

Keywords: Polynomial chaos; Uncertainty; Fluids; Stochastic modeling

1. Introduction

Recently there has been an intense interest in verification and validation of large-scale simulations and in modeling uncertainty [1–3]. In simulations, just like in the experiments, we often question the accuracy of the results and we construct a posteriori error bounds, but the new objective is to model the uncertainty from the beginning of the simulations and not simply as an afterthought. Numerical accuracy and error control have been employed in simulations for some time now, at least for the modern discretizations, e.g.

* Corresponding author. Fax: 1-401-863-3369.
E-mail address: gk@dam.brown.edu (G.E. Karniadakis).

0021-9991/03/$ - see front matter
doi:10.1016/S0021-9991(03)00092-5

[4,5]. However, there are always some uncertain components associated with the physical problems, specifically with such diverse factors as constitutive laws, boundary and initial conditions, transport coefficients, source and interaction terms, geometric irregularities (e.g., roughness), etc.

Most of the research efforts in CFD research so far have been in developing efficient algorithms for different applications, assuming ideal inputs with precisely defined computational domains. With the field reaching some degree of maturity now, we naturally pose the more general question of how to model uncertainty and stochastic inputs, and how to formulate algorithms to accurately reflect the propagation of the uncertainty. To this end, the Monte Carlo approach can be employed but it is computationally expensive and is only used as the last resort. The sensitivity method is a more economical approach, based on the moments of samples, but it is less robust and depends strongly on the modeling assumptions [6]. One popular technique is the perturbation method where all the stochastic quantities are expanded around their mean via Taylor series. This approach, however, is limited to small perturbations and does not readily provide information on high-order statistics of the response. The resulting system of equations becomes extremely complicated beyond second-order expansion. Another approach is based on expanding the inverse of the stochastic operator in a Neumann series, but this too is limited to small fluctuations, and even combinations with the Monte Carlo method seem to result in computationally prohibitive algorithms for complex systems [7].

A more effective approach pioneered by Ghanem and Spanos [8] in the context of finite elements for solid mechanics is based on a spectral representation of the uncertainty. This allows high-order representation, not just first-order as in most perturbation-based methods, at high computational efficiency. It is based on the original theory of Wiener [9,10] on homogeneous chaos. This approach was employed in turbulence in the 1960s [11–13]. However, it was realized that the chaos expansion converges slowly for turbulent field [14–16], so polynomial chaos did not receive much attention for a long time.

The main purpose of this paper is to demonstrate that the polynomial chaos expansion can be effective in modeling uncertainties associated with fluid flows. When the uncertainty has relatively strong correlation, the chaos expansion converges fast; in the ideal case it converges exponentially fast due to the fact that it is a spectral expansion in the random space. The spectral representation of the uncertainty is based on a trial basis $\{\Psi(\boldsymbol{\xi}(\theta))\}$ where θ denotes the random event. For example, the vorticity has the following finite-dimensional representation:

$$\omega(\mathbf{x},t,\theta) = \sum_{i=0}^{P} \omega_i(\mathbf{x},t)\Psi_i(\boldsymbol{\xi}(\theta)).$$

Here $\omega_i(\mathbf{x},t)$ represents the deterministic coefficients and will be denoted as the random mode (i) of the vorticity. The random trial basis is a set of complete orthogonal polynomials in terms of the multi-dimensional random variable $\boldsymbol{\xi}(\theta)$ with a specific probability distribution. $\Psi(\boldsymbol{\xi}(\theta))$ is a functional, as it is a function of random variables $\boldsymbol{\xi}$ which are functions of the random parameter $\theta \in [0,1]$. For the original polynomial chaos introduced by Wiener, the polynomial trial basis is the *Hermite* polynomials in terms of multi-dimensional *Gaussian* random variables. In this paper, we will apply this expansion to fluid flows and further generalize the trial basis to other orthogonal polynomials from the Askey scheme [17]. For different types of basis polynomials, the random variables $\boldsymbol{\xi}(\theta)$ are not restricted to the Gaussian variables. Therefore, we have additional flexibility to represent the non-Gaussian processes more efficiently. The theory of orthogonal functionals plays a key role in the algorithms developed here. We note that the Monte Carlo algorithm can be thought of as a subcase of the above representation corresponding to the collocation procedure where the test basis is $\Psi_i(\theta) = \delta(\theta - \theta_i)$, where δ is the Kronecker delta function and θ_i refers to an isolated random event.

The algorithms we develop here are general but we present applications with uncertainty associated with boundary conditions. This situation is encountered, for example, in micro-channel flows but also in clas-

sical flows such as the freestream flow past bluff bodies. The generalized polynomial chaos expansion can handle both Gaussian and non-Gaussian random processes. For certain distributions there exist a "best" representation which results in fast convergence rate. For example, for Poisson distributions is the Charlier polynomials, for Gamma distributions the Laugerre polynomials, for binomial distributions the Krawtchouk polynomials, for the beta distributions the Jacobi polynomials, etc.

In the next section we review the theory of the Askey scheme of hypergeometric orthogonal polynomials, and in Section 3 we present the framework of the generalized polynomial chaos. In Section 4 we address its implementation details when applied to Navier–Stokes equations. In Section 5 we present the computational results of various applications and demonstrate the convergence property of the chaos expansion. We conclude the paper with a discussion on open questions. In Appendix A we include a brief review of orthogonal polynomials.

2. The Askey scheme of hypergeometric orthogonal polynomials

The theory of orthogonal polynomials is relatively mature and several books have been devoted to their study (e.g. [18–20]). More recent work has shown that an important class of orthogonal polynomials belongs to the Askey scheme of the hypergeometric polynomials [17]. In this section, we briefly review the theory of hypergeometric orthogonal polynomials; we adopt the notation of Koekoek and Swarttouw [21] and Schoutens [22].

2.1. The generalized hypergeometric series

We first introduce the *Pochhammer symbol* $(a)_n$ defined by

$$(a)_n = \begin{cases} 1 & \text{if } n = 0, \\ a(a+1)\cdots(a+n-1) & \text{if } n = 1,2,3,\ldots \end{cases} \tag{1}$$

In terms of Gamma function, we have

$$(a)_n = \frac{\Gamma(a+n)}{\Gamma(a)}, \qquad n > 0. \tag{2}$$

The *generalized hypergeometric series* ${}_rF_s$ is defined by

$${}_rF_s(a_1,\ldots,a_r;b_1,\ldots,b_s;z) = \sum_{k=0}^{\infty} \frac{(a_1)_k \cdots (a_r)_k}{(b_1)_k \cdots (b_s)_k} \frac{z^k}{k!}, \tag{3}$$

where $b_i \neq 0, -1, -2, \ldots$ for $i = \{1,\ldots,s\}$ to ensure the denominator factors in the terms of the series are never zero. The radius of convergence ρ of the hypergeometric series is

$$\rho = \begin{cases} \infty & \text{if } r < s+1, \\ 1 & \text{if } r = s+1, \\ 0 & \text{if } r > s+1. \end{cases} \tag{4}$$

Some elementary cases of the hypergeometric series are: the exponential series ${}_0F_0$ and the binomial series ${}_1F_0$.

If one of the numerator parameters $a_i,\ i = 1,\ldots,r$, is a negative integer, say $a_1 = -n$, the hypergeometric series (3) terminates at the nth-term and becomes a polynomial in z,

$$ {}_rF_s(-n,\ldots,a_r;b_1,\ldots,b_s;z)=\sum_{k=0}^{n}\frac{(-n)_k\cdots(a_r)_k}{(b_1)_k\cdots(b_s)_k}\frac{z^k}{k!}. \tag{5} $$

2.2. Some properties of the orthogonal polynomials

A system of polynomials $\{Q_n(x),\ n\in\mathcal{N}\}$ where $Q_n(x)$ is a polynomial of exact degree n and $\mathcal{N}=\{0,1,2,\ldots\}$ or $\mathcal{N}=\{0,1,\ldots,N\}$ for a finite nonnegative integer N, is an orthogonal system of polynomials with respect to some real positive measure ϕ if the following orthogonality relations are satisfied:

$$ \int_S Q_n(x)Q_m(x)\,\mathrm{d}\phi(x)=h_n^2\delta_{nm},\quad n,m\in\mathcal{N}, \tag{6} $$

where S is the support of the measure ϕ and the h_n are non-zero constants. The system is called orthonormal if $h_n=1$.

The measure ϕ often has a density $w(x)$ or weights $w(i)$ at points x_i in the discrete case. The relations (6) then become

$$ \int_S Q_n(x)Q_m(x)w(x)\,\mathrm{d}x=h_n^2\delta_{nm},\quad n,m\in\mathcal{N}, \tag{7} $$

in the continuous case, or

$$ \sum_{i=0}^{M}Q_n(x_i)Q_m(x_i)w(x_i)=h_n^2\delta_{nm},\quad n,m\in\mathcal{N}, \tag{8} $$

in the discrete case where it is possible that $M=\infty$.

The density $w(x)$, or weights $w(i)$ in the discrete case, is also commonly referred as the *weighting function* in the theory of orthogonal polynomials. It will be shown later that the weighting functions for some orthogonal polynomials are identical to certain probability functions. For example, the weighting function for the Hermite polynomials is the same as probability density function of the Gaussian random variables. This fact plays an important role in representing stochastic processes with orthogonal polynomials.

2.3. The Askey scheme

The Askey scheme, which is represented as a tree structure in Fig. 1 (following [22]), classifies the hypergeometric orthogonal polynomials and indicates the limit relations between them. The 'tree' starts with the Wilson polynomials and the Racah polynomials on the top. They both belong to the class ${}_4F_3$ of the hypergeometric orthogonal polynomials given by Eq. (5). The Wilson polynomials are continuous while the Racah polynomials are discrete. The lines connecting different polynomials denote the limit transition relationships between them; this implies that the polynomials at the lower end of the lines can be obtained by taking the limit of one of the parameters from their counterparts on the upper end. For example, the limit relation between Jacobi polynomials $P_n^{(\alpha,\beta)}(x)$ and Hermite polynomials $H_n(x)$ is

$$ \lim_{\alpha\to\infty}\alpha^{-1/2n}P_n^{(\alpha,\alpha)}\left(\frac{x}{\sqrt{\alpha}}\right)=\frac{H_n(x)}{2^n n!}, $$

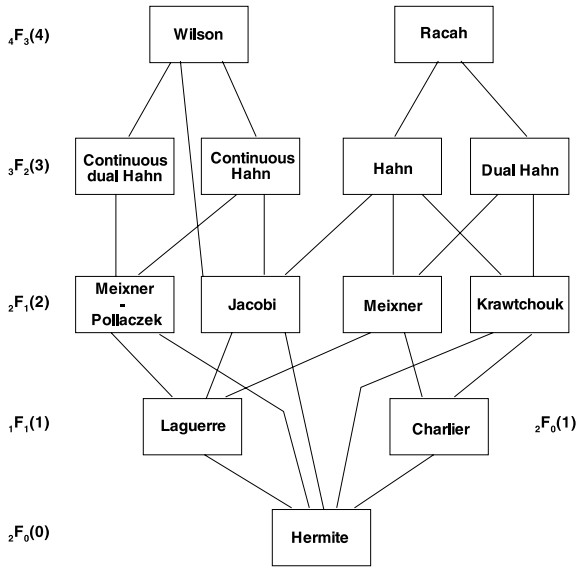

Fig. 1. The Askey scheme of orthogonal polynomials.

and between Meixner polynomials $M_n(x;\beta,c)$ and Charlier polynomials $C_n(x;a)$ is

$$\lim_{\beta\to\infty} M_n\left(x;\beta,\frac{a}{a+\beta}\right) = C_n(x;a).$$

For a detailed account of the limit relations of Askey scheme, the interested reader should consult Koekoek and Swarttouw [21] and Schoutens [22].

The orthogonal polynomials associated with the generalized polynomial chaos, which will also be called the Askey-chaos hereafter, include: Hermite, Laguerre, Jacobi, Charlier, Meixner, Krawtchouk and Hahn polynomials. A review of their definitions and properties can be found in Appendix A of this paper.

3. The generalized polynomial chaos

In this section we introduce the generalized polynomial chaos expansion along with the Karhunen–Loeve (KL) expansion, another classical technique for representing random processes. The KL expansion can be used in some cases to represent efficiently the known stochastic fields, i.e., the stochastic inputs.

3.1. The original Wiener polynomial chaos: Hermite-chaos

The original polynomial chaos, also termed as the homogeneous chaos, was first introduced by Wiener [9]. It employs the *Hermite* polynomials in terms of *Gaussian* random variables. According to a theorem by Cameron and Martin [23], it can approximate any functionals in $L_2(C)$ and converges in the $L_2(C)$ sense, where C is the space of real functions which are continuous on the interval $[0,1]$ and vanish at 0. Therefore, polynomial chaos provides a means for expanding second-order random processes in terms of Hermite polynomials. Second-order random processes are processes with finite variance, and this applies to most physical processes. Thus, a general second-order random process $X(\theta)$, viewed as a function of θ, i.e., the random event, can be represented in the form

$$X(\theta) = a_0 H_0 + \sum_{i_1=1}^{\infty} a_{i_1} H_1(\xi_{i_1}(\theta)) + \sum_{i_1=1}^{\infty} \sum_{i_2=1}^{i_1} a_{i_1 i_2} H_2(\xi_{i_1}(\theta), \xi_{i_2}(\theta)) + \sum_{i_1=1}^{\infty} \sum_{i_2=1}^{i_1} \sum_{i_3=1}^{i_2} a_{i_1 i_2 i_3} H_3(\xi_{i_1}(\theta), \xi_{i_2}(\theta), \xi_{i_3}(\theta)) + \cdots, \tag{9}$$

where $H_n(\xi_{i_1}, \ldots, \xi_{i_n})$ denote the *Hermite* polynomials of order n in terms of the multi-dimensional independent standard *Gaussian* random variables $\boldsymbol{\xi} = (\xi_{i_1}, \ldots, \xi_{i_n})$ with zero mean and unit variance. The above equation is the discrete version of the original Wiener polynomial chaos expansion, where the continuous integrals are replaced by summations. The general expression of the Hermite polynomials is given by

$$H_n(\xi_{i_1}, \ldots, \xi_{i_n}) = \mathrm{e}^{1/2\boldsymbol{\xi}^T\boldsymbol{\xi}}(-1)^n \frac{\partial^n}{\partial\xi_{i_1} \cdots \partial\xi_{i_n}} \mathrm{e}^{-1/2\boldsymbol{\xi}^T\boldsymbol{\xi}}. \tag{10}$$

For example, the one-dimensional Hermite polynomials are:

$$\Psi_0 = 1, \quad \Psi_1 = \xi, \quad \Psi_2 = \xi^2 - 1, \quad \Psi_3 = \xi^3 - 3\xi, \quad \ldots \tag{11}$$

For notational convenience, Eq. (9) can be rewritten as

$$X(\theta) = \sum_{j=0}^{\infty} \hat{a}_j \Psi_j(\boldsymbol{\xi}), \tag{12}$$

where there is a one-to-one correspondence between the functions $H_n(\xi_{i_1}, \ldots, \xi_{i_n})$ and $\Psi_j(\boldsymbol{\xi})$, and also between the coefficients $\hat{a}_j$ and $a_{i_1,\ldots,i_r}$. In Eq. (9) the summation is carried out according to the order of the Hermite polynomials, while in Eq. (12) it is simply a re-numbering with the polynomials of lower order counted first. For clarity, the two-dimensional expansion is shown here, both in the fully expanded form (see Eq. (9))

$$X(\theta) = a_0 H_0 + a_1 H_1(\xi_1) + a_2 H_1(\xi_2) + a_{11} H_2(\xi_1, \xi_1) + a_{12} H_2(\xi_2, \xi_1) + a_{22} H_2(\xi_2, \xi_2) + \cdots, \tag{13}$$

and the simplified form (see Eq. (12))

$$\begin{aligned} X(\theta) &= \hat{a}_0 \Psi_0 + \hat{a}_1 \Psi_1 + \hat{a}_2 \Psi_2 + \hat{a}_3 \Psi_3 + \hat{a}_3 \Psi_4 + \hat{a}_5 \Psi_5 + \cdots \\ &= \hat{a}_0 + \hat{a}_1 \xi_1 + \hat{a}_2 \xi_2 + \hat{a}_3(\xi_1^2 - 1) + \hat{a}_3(\xi_1 \xi_2) + \hat{a}_5(\xi_2^2 - 1) + \cdots \end{aligned} \tag{14}$$

The polynomial chaos forms a complete *orthogonal* basis in the L_2 space of the Gaussian random variables, i.e.,

$$\langle \Psi_i \Psi_j \rangle = \langle \Psi_i^2 \rangle \delta_{ij}, \tag{15}$$

where δ_{ij} is the Kronecker delta and $\langle \cdot, \cdot \rangle$ denotes the ensemble average. This is the inner product in the Hilbert space of the Gaussian random variables

$$\langle f(\boldsymbol{\xi}) g(\boldsymbol{\xi}) \rangle = \int f(\boldsymbol{\xi}) g(\boldsymbol{\xi}) W(\boldsymbol{\xi}) \, \mathrm{d}\boldsymbol{\xi}. \tag{16}$$

The weighting function is

$$W(\boldsymbol{\xi}) = \frac{1}{\sqrt{(2\pi)^n}} \mathrm{e}^{-1/2\boldsymbol{\xi}^T\boldsymbol{\xi}}, \tag{17}$$

where n is the dimension of $\boldsymbol{\xi}$. What distinguishes the Wiener–Hermite expansion from many other possible complete sets of expansions is that the polynomials here are orthogonal with respect to the weighting function $W(\boldsymbol{\xi})$ which has the form of the multi-dimensional independent Gaussian probability distribution with unit variance. We will use the term Hermite-chaos hereafter to denote the Wiener polynomial chaos.

3.2. The generalized polynomial chaos: Askey-chaos

The Hermite-chaos expansion has been quite effective in solving stochastic differential equations with Gaussian inputs as well as certain types of non-Gaussian inputs, e.g., lognormal distributions [8,24,25]; this can be justified by the Cameron–Martin theorem [23]. However, for general non-Gaussian random inputs, the convergence rate is not fast. In some cases the convergence rate is, in fact, severely deteriorated.

In order to deal with more general random inputs, we introduce the generalized polynomial chaos expansion, the *Askey-chaos*, as a generalization of the original Wiener's Hermite-chaos expansion. The expansion basis of the Askey-chaos is formed by the complete set of orthogonal polynomials from the Askey scheme (see Section 2.3). Similar to Section 3.1, we represent the general second-order random process $X(\theta)$ as

$$\begin{aligned} X(\theta) = a_0 I_0 + \sum_{i_1=1}^{\infty} c_{i_1} I_1(\zeta_{i_1}(\theta)) + \sum_{i_1=1}^{\infty} \sum_{i_2=1}^{i_1} c_{i_1 i_2} I_2(\zeta_{i_1}(\theta), \zeta_{i_2}(\theta)) \\ + \sum_{i_1=1}^{\infty} \sum_{i_2=1}^{i_1} \sum_{i_3=1}^{i_2} c_{i_1 i_2 i_3} I_3(\zeta_{i_1}(\theta), \zeta_{i_2}(\theta), \zeta_{i_3}(\theta)) + \cdots, \end{aligned} \tag{18}$$

where $I_n(\zeta_{i_1}, \ldots, \zeta_{i_n})$ denotes the Askey-chaos of order n in terms of the multi-dimensional random variables $\boldsymbol{\zeta} = (\zeta_{i_1}, \ldots, \zeta_{i_n})$. In the Askey-chaos expansion, the polynomials I_n are not restricted to Hermite polynomials but instead they could be any member of the Askey scheme, as shown in Fig. 1. Again for notational convenience, we rewrite Eq. (18) as

$$X(\theta) = \sum_{j=0}^{\infty} \hat{c}_j \Phi_j(\boldsymbol{\zeta}), \tag{19}$$

where there is a one-to-one correspondence between the functions $I_n(\zeta_{i_1}, \ldots, \zeta_{i_n})$ and $\Phi_j(\boldsymbol{\zeta})$, and their coefficients $\hat{c}_j$ and $c_{i_1,\ldots,i_r}$. Since each type of polynomials from the Askey scheme form a complete basis in the Hilbert space determined by their corresponding support, we can expect each type of Askey-chaos to converge to any L_2 functional in the L_2 sense in the corresponding Hilbert functional space as a generalized result of Cameron–Martin theorem [23,26]. The orthogonality relation of the Askey-chaos polynomial chaos takes the form

$$\langle \Phi_i \Phi_j \rangle = \langle \Phi_i^2 \rangle \delta_{ij}, \tag{20}$$

where δ_{ij} is the Kronecker delta and $\langle \cdot, \cdot \rangle$ denotes the ensemble average which is the inner product in the Hilbert space of the variables $\boldsymbol{\zeta}$

$$\langle f(\boldsymbol{\zeta}) g(\boldsymbol{\zeta}) \rangle = \int f(\boldsymbol{\zeta}) g(\boldsymbol{\zeta}) W(\boldsymbol{\zeta}) \, \mathrm{d}\boldsymbol{\zeta}, \tag{21}$$

or

$$\langle f(\boldsymbol{\zeta}) g(\boldsymbol{\zeta}) \rangle = \sum_{\boldsymbol{\zeta}} f(\boldsymbol{\zeta}) g(\boldsymbol{\zeta}) W(\boldsymbol{\zeta}) \tag{22}$$

Table 1
Correspondence of the type of Wiener–Askey polynomial chaos to the type of random inputs ($N \geqslant 0$ is a finite integer)

	Random inputs	Wiener–Askey chaos	Support
Continuous	Gaussian	Hermite-chaos	$(-\infty, \infty)$
	Gamma	Laguerre-chaos	$[0, \infty)$
	Beta	Jacobi-chaos	$[a, b]$
	Uniform	Legendre-chaos	$[a, b]$
Discrete	Poisson	Charlier-chaos	$\{0, 1, 2, \ldots\}$
	Binomial	Krawtchouk-chaos	$\{0, 1, \ldots, N\}$
	Negative binomial	Meixner-chaos	$\{0, 1, 2, \ldots\}$
	Hypergeometric	Hahn-chaos	$\{0, 1, \ldots, N\}$

in the discrete case. Here $W(\boldsymbol{\zeta})$ is the weighting function corresponding to the Askey polynomials chaos basis $\{\Phi_i\}$; see Appendix A for detailed formulas. Some types of orthogonal polynomials from the Askey scheme have weighting functions of the same form as the probability function of certain types of random distributions. In practice, we then choose the type of independent variables $\boldsymbol{\zeta}$ in the polynomials $\{\Phi_i(\boldsymbol{\zeta})\}$ according to the type of random distributions as shown in Table 1. It is clear that the original Wiener polynomial chaos corresponds to the Hermite-chaos and is a subset of the Askey-chaos. The Hermite-, Laguerre- and Jacobi-chaos are *continuous chaos*, while Charlier-, Meixner-, Krawtchouk- and Hahn-chaos are *discrete chaos*. It is worth mentioning that the Legendre polynomials, which is a special case of the Jacobi polynomials $P_n^{(\alpha,\beta)}(x)$ with parameters $\alpha = \beta = 0$, correspond to an important distribution – the *uniform distribution*. Due to the importance of the uniform distribution, we list it separately in the table and term the corresponding chaos expansion as the Legendre-chaos.

3.3. The Karhunen–Loeve expansion

The Karhunen–Loeve (KL) expansion [27] is another way of representing a random process. It is based on the spectral expansion of the covariance function of the process. Let us denote the process by $h(\mathbf{x}, \theta)$ and its covariance function by $R_{hh}(\mathbf{x}, \mathbf{y})$, where $\mathbf{x}$ and $\mathbf{y}$ are the spatial or temporal coordinates. By definition, the covariance function is real, symmetric, and positive definite. All eigenfunctions are mutually orthogonal and form a complete set spanning the function space to which $h(\mathbf{x}, \theta)$ belongs. The KL expansion then takes the following form:

$$h(\mathbf{x}, \theta) = \bar{h}(\mathbf{x}) + \sum_{i=1}^{\infty} \sqrt{\lambda_i}\phi_i(\mathbf{x})\xi_i(\theta), \tag{23}$$

where $\bar{h}(\mathbf{x})$ denotes the mean of the random process, and $\xi_i(\theta)$ forms a set of uncorrelated random variables. Also, $\phi_i(\mathbf{x})$ and λ_i are the eigenfunctions and eigenvalues of the covariance function, respectively, i.e.,

$$\int R_{hh}(\mathbf{x}, \mathbf{y})\phi_i(\mathbf{y})\,\mathrm{d}\mathbf{y} = \lambda_i\phi_i(\mathbf{x}). \tag{24}$$

Among many possible decompositions of a random process, the KL expansion is optimal in the sense that the mean-square error of the finite representation of the process is minimized. Its use, however, is limited as the covariance function of the solution process is often not known a priori. Nevertheless, the KL expansion provides an effective means of representing the input random processes when the covariance structure is known.

4. The Askey-chaos for Navier–Stokes equations

In this section we present the solution procedure for solving the stochastic Navier–Stokes equations by generalized polynomial chaos expansion. The randomness in the solution can be introduced through boundary conditions, initial conditions, forcing, etc.

4.1. Governing equations

We employ the incompressible Navier–Stokes equations:

$$\nabla \cdot \mathbf{u} = 0, \tag{25}$$

$$\frac{\partial \mathbf{u}}{\partial t} + (\mathbf{u} \cdot \nabla)\mathbf{u} = -\nabla \Pi + Re^{-1}\nabla^2 \mathbf{u}, \tag{26}$$

where Π is the pressure and Re the Reynolds number. All flow quantities, i.e., velocity and pressure are considered stochastic processes. A random dimension, denoted by the parameter θ, is introduced in addition to the spatial–temporal dimensions $(\mathbf{x}, t)$, thus

$$\mathbf{u} = \mathbf{u}(\mathbf{x}, t; \theta); \quad \Pi = \Pi(\mathbf{x}, t; \theta). \tag{27}$$

We then apply the generalized polynomial chaos expansion, or the Askey-chaos (19), to these quantities and obtain

$$\mathbf{u}(\mathbf{x}, t; \theta) = \sum_{i=0}^{P} \mathbf{u}_i(\mathbf{x}, t)\Phi_i(\boldsymbol{\zeta}(\theta)); \quad \Pi(\mathbf{x}, t; \theta) = \sum_{i=0}^{P} \Pi_i(\mathbf{x}, t)\Phi_i(\boldsymbol{\zeta}(\theta)), \tag{28}$$

where we have replaced the infinite summation in infinite dimension of $\boldsymbol{\zeta}$ in Eq. (12) by a truncated finite-term summation in finite dimensional space of $\boldsymbol{\zeta}$. The total number of expansion terms, $(P+1)$, depends on the number of random dimensions (n) of $\boldsymbol{\zeta}$ and the highest order (p) of the polynomials Φ [8]

$$P = \sum_{s=1}^{p} \frac{1}{s!} \prod_{r=0}^{s-1} (n + r). \tag{29}$$

The most important aspect of the above expansion is that the random processes have been decomposed into a set of deterministic functions in the spatial–temporal variables multiplied by the random basis polynomials which are independent of these variables.

Substituting (28) into Navier–Stokes equations (25) and (26) and noting that the partial derivatives are taken in physical space and thus commute with the operations in random space, we obtain the following equations:

$$\sum_{i=0}^{P} \nabla \cdot \mathbf{u}_i(\mathbf{x}, t)\Phi_i = 0, \tag{30}$$

$$\sum_{i=0}^{P} \frac{\partial \mathbf{u}_i(\mathbf{x}, t)}{\partial t}\Phi_i + \sum_{i=0}^{P}\sum_{j=0}^{P}[(\mathbf{u}_i \cdot \nabla)\mathbf{u}_j)]\Phi_i\Phi_j = -\sum_{i=0}^{P} \nabla \Pi_i(\mathbf{x}, t)\Phi_i + Re^{-1}\sum_{i=0}^{P} \nabla^2 \mathbf{u}_i \Phi_i. \tag{31}$$

We then project the above equations onto the random space spanned by the basis polynomials $\{\Phi_i\}$ by taking the inner product of above equation with each basis. By taking $\langle \cdot, \Phi_k \rangle$ and utilizing the orthogonality condition (15), we obtain the following set of equations:

For each $k = 0, \ldots, P$,

$$\nabla \cdot \mathbf{u}_k = 0, \tag{32}$$

$$\frac{\partial \mathbf{u}_k}{\partial t} + \frac{1}{\langle \Phi_k^2 \rangle} \sum_{i=0}^{P} \sum_{j=0}^{P} e_{ijk}[(\mathbf{u}_i \cdot \nabla)\mathbf{u}_j)] = -\nabla \Pi_k + Re^{-1} \nabla^2 \mathbf{u}_k, \tag{33}$$

where $e_{ijk} = \langle \Phi_i \Phi_j \Phi_k \rangle$. Together with $\langle \Phi_i^2 \rangle$, the coefficients e_{ijk} can be evaluated analytically from the definition of Φ_i. The set of equations consists of $(P+1)$ system of 'Navier–Stokes-like' equations for each random mode coupled through the convective terms.

4.2. Numerical formulation

4.2.1. Temporal discretization

We employ the semi-implicit high-order fractional step method, which for the standard deterministic Navier–Stokes equations (25) and (26) has the form [28]:

$$\frac{\hat{\mathbf{u}} - \sum_{q=0}^{J} \alpha_q \mathbf{u}^{n-q}}{\Delta t} = -\sum_{q=0}^{J} \beta_q [(\mathbf{u} \cdot \nabla)\mathbf{u}]^{n-q}, \tag{34}$$

$$\frac{\hat{\hat{\mathbf{u}}} - \hat{\mathbf{u}}}{\Delta t} = -\nabla \Pi^{n+1}, \tag{35}$$

$$\frac{\gamma_0 \mathbf{u}^{n+1} - \hat{\hat{\mathbf{u}}}}{\Delta t} = Re^{-1} \nabla^2 \mathbf{u}^{n+1}, \tag{36}$$

where J is order of accuracy in time and α, β and γ are integration weights. A pressure Poisson equation is obtained by enforcing the discrete divergence-free condition $\nabla \cdot \mathbf{u}^{n+1} = 0$

$$\nabla^2 \Pi^{n+1} = \frac{1}{\Delta t} \nabla \cdot \hat{\mathbf{u}} \tag{37}$$

with the appropriate pressure boundary condition given as

$$\frac{\partial \Pi}{\partial n} = \mathbf{n} \cdot \left[\hat{\mathbf{u}}/\Delta t - Re^{-1} \nabla \times \boldsymbol{\omega}^{n+1} \right], \tag{38}$$

where $\mathbf{n}$ is the outward unit normal vector and $\boldsymbol{\omega} = \nabla \times \mathbf{u}$ is the vorticity. The method achieves third-order accuracy in time; the coefficients for the integration weights can be found in [29].

In order to discretize the stochastic Navier–Stokes equations, we apply the same approach to the coupled set of equations (32) and (33):

For each $k = 0, \ldots, P$,

$$\frac{\hat{\mathbf{u}}_k - \sum_{q=0}^{J} \alpha_q \mathbf{u}_k^{n-q}}{\Delta t} = -\frac{1}{\langle \Phi_k^2 \rangle} \sum_{q=0}^{J} \beta_q \left[\sum_{i=0}^{P} \sum_{j=0}^{P} e_{ijk} (\mathbf{u}_i \cdot \nabla)\mathbf{u}_j \right]^{n-q}, \tag{39}$$

$$\frac{\hat{\hat{\mathbf{u}}}_k - \hat{\mathbf{u}}_k}{\Delta t} = -\nabla \Pi_k^{n+1}, \tag{40}$$

$$\frac{\gamma_0 \mathbf{u}_k^{n+1} - \hat{\hat{\mathbf{u}}}_k}{\Delta t} = Re^{-1} \nabla^2 \mathbf{u}_k^{n+1}. \tag{41}$$

The discrete divergence-free condition for each mode $\nabla \cdot \mathbf{u}_k^{n+1} = 0$ results in a set of consistent Poisson equations for each pressure mode

$$\nabla^2 \Pi_k^{n+1} = \frac{1}{\Delta t} \nabla \cdot \hat{\mathbf{u}}_k, \quad k = 0, \ldots, P, \tag{42}$$

with appropriate pressure boundary condition derived similarly as in [28]

$$\frac{\partial \Pi_k}{\partial n} = \mathbf{n} \cdot \left[\hat{\mathbf{u}}_k / \Delta t - Re^{-1} \nabla \times \boldsymbol{\omega}_k^{n+1} \right], \quad k = 0, \ldots, P, \tag{43}$$

where $\mathbf{n}$ is the outward unit normal vector along the boundary, and $\boldsymbol{\omega}_k = \nabla \times \mathbf{u}_k$ is the vorticity for each random mode.

4.2.2. Spatial discretization

Spatial discretization can be carried out by any method, but here we employ the spectral/*hp* element method in order to have better control of the numerical error [29]. In addition, the all-spectral discretization in space and along the random direction leads to homogeneous inner products, which in turn results in more efficient ways of inverting the algebraic systems. In particular, the spatial discretization is based on Jacobi polynomials on triangles or quadrilaterals in two dimensions, and tetrahedra, hexahedra or prisms in three dimensions.

4.3. Post-processing

The coefficients in the expansion of the solution process (Eq. (28)) are obtained after solving Eqs. (39)–(43). We then obtain the analytical form (in random space) of the solution process. It is possible to perform a number of analytical operations on the stochastic solution in order to carry out other analysis such as the sensitivity analysis. Specifically, the *mean* solution is contained in the expansion term with index of zero. The *second-moment*, i.e., the *covariance function* is given by

$$R_{\mathbf{uu}}(\mathbf{x}_1, t_1; \mathbf{x}_2, t_2) = \langle \mathbf{u}(\mathbf{x}_1, t_1) - \overline{\mathbf{u}(\mathbf{x}_1, t_1)}, \mathbf{u}(\mathbf{x}_2, t_2) - \overline{\mathbf{u}(\mathbf{x}_2, t_2)} \rangle = \sum_{i=1}^{P} \left[\mathbf{u}_i(\mathbf{x}_1, t_1) \mathbf{u}_i(\mathbf{x}_2, t_2) \langle \Phi_i^2 \rangle \right]. \tag{44}$$

Note that the summation starts from index $(i = 1)$ instead of 0 to exclude the mean, and that the orthogonality of the Askey-chaos basis $\{\Phi_i\}$ has been used in deriving the above equation. The *variance* of the solution, i.e., the 'mean-square' value, is obtained as

$$\mathrm{Var}(\mathbf{u}(\mathbf{x}, t)) = \left\langle \left(\mathbf{u}(\mathbf{x}, t) - \overline{\mathbf{u}(\mathbf{x}, t)} \right)^2 \right\rangle = \sum_{i=1}^{P} \left[\mathbf{u}_i^2(\mathbf{x}, t) \langle \Phi_i^2 \rangle \right], \tag{45}$$

and the root-mean-square (rms) is simply the square root of the variance. Similar expressions can be obtained for the pressure field.

5. Numerical results

In this section we present numerical results of the applications of the generalized polynomial chaos. We first consider the stochastic ordinary differential equation and demonstrate exponential convergence with the optimal Askey-chaos. We then solve the incompressible flow in the pressure-driven channel where there is uncertainty associated with the wall boundary conditions. Subsequently, we simulate laminar flow past a circular cylinder with uncertain freestream.

5.1. Stochastic ordinary differential equation

5.1.1. Solution procedure

To demonstrate the convergence type, we consider the ordinary differential equation

$$\frac{\mathrm{d}y(t)}{\mathrm{d}t} = -ky, \quad y(0) = \hat{y}, \tag{46}$$

where the decay rate coefficient k is considered to be a random variable $k(\theta)$ with certain distribution and zero mean value $\bar{k} = 0$. The probability function is $f(k)$ for the continuous case or $f(k_i)$ for the discrete case. The *deterministic* solution is constant over time $y(t) = \hat{y}\mathrm{e}^{-\bar{k}t} = \hat{y}$, while the *mean* of *stochastic* solution is

$$\bar{y}(t) = \hat{y}\int_S \mathrm{e}^{-kt} f(k)\,\mathrm{d}k \quad \text{or} \quad \bar{y}(t) = \hat{y}\sum_i \mathrm{e}^{-k_i t} f(k_i) \tag{47}$$

corresponding to the continuous and discrete distributions, respectively. The integration and summation are taken within the support of the corresponding distribution, and in general the mean of stochastic solution is time varying.

By applying the generalized polynomial chaos expansion of Eq. (19) to the solution y and random input k

$$y(t) = \sum_{i=0}^{P} y_i(t)\Phi_i, \quad k = \sum_{i=0}^{P} k_i\Phi_i \tag{48}$$

and substituting the expansions into the governing equation, we obtain

$$\sum_{i=0}^{P} \frac{\mathrm{d}y_i(t)}{\mathrm{d}t}\Phi_i = -\sum_{i=0}^{P}\sum_{j=0}^{P} \Phi_i\Phi_j k_i y_j(t). \tag{49}$$

A Galerkin projection onto each polynomial basis results in a set of coupled ordinary differential equations for each random mode

$$\frac{\mathrm{d}y_l(t)}{\mathrm{d}t} = -\frac{1}{\langle\Phi_l^2\rangle}\sum_{i=0}^{P}\sum_{j=0}^{P} e_{ijl}k_i y_j(t), \quad l = 0, 1, \ldots, P, \tag{50}$$

where $e_{ijl} = \langle\Phi_i\Phi_j\Phi_l\rangle$. A standard second-order Runge–Kutta scheme is used to integrate the equations. We define the two error measures for the mean and variance of the solution:

$$\varepsilon_{\mathrm{mean}}(t) = \left|\frac{\bar{y}(t) - \bar{y}_{\mathrm{exact}}(t)}{\bar{y}_{\mathrm{exact}}(t)}\right|, \quad \varepsilon_{\mathrm{var}}(t) = \left|\frac{\sigma^2(t) - \sigma^2_{\mathrm{exact}}(t)}{\sigma^2_{\mathrm{exact}}(t)}\right|, \tag{51}$$

where $\bar{y}(t) = E[y(t)]$ is the mean value of $y(t)$ and $\sigma^2(t) = E[(y(t) - \bar{y}(t))^2]$ is the variance of the solution. The initial condition is fixed to be $\hat{y} = 1$ and the integration is performed up to $t = 1$ (non-dimensional time units).

5.1.2. Gaussian distribution and Hermite-chaos

When k is a Gaussian random variable with probability density function $f(k) = 1/\sqrt{2\pi}e^{-k^2/2}$, the optimal Askey-chaos is the Hermite-chaos which can represent the input k 'exactly' with first-order expansion. Fig. 2 shows the solution by the Hermite-chaos expansion. The convergence to zero of errors in the mean and variance as the order of Hermite-chaos increases is shown on semi-log plot; *exponential* convergence rate is achieved.

5.1.3. Poisson distribution and Charlier-chaos

As an example of the discrete case, we assume k is a random variable with *Poisson* distribution

$$f(k;\lambda) = e^{-\lambda}\frac{\lambda^k}{k!}, \quad k = 0, 1, 2, \ldots, \lambda > 0. \tag{52}$$

In this case the optimal Askey-chaos is the Charlier-chaos (see Table 1).

Results with fourth-order Charlier-chaos expansion are shown in Fig. 3 for two different distributions corresponding to different values of λ. Again, exponential convergence rate is observed.

5.1.4. Effects of non-optimal basis

In this section we present examples of representing a stochastic input with non-optimal Askey-chaos. More specifically, we present results of using Hermite-chaos expansion for an exponential distribution. Although, in theory, Hermite-chaos converges and it has been successfully applied to some non-Gaussian processes (e.g., lognormal [24]), we demonstrate numerically here that exponential convergence rate is not realized. In Fig. 4 the approximation of an exponential random variable by Hermite-chaos is plotted on the left. It can be seen the Hermite-chaos converges and the fifth-order approximation is very close to the exact distribution, with some noticeable difference at $x \sim 0$ where the PDF reaches its peak at 1. Subsequently, if

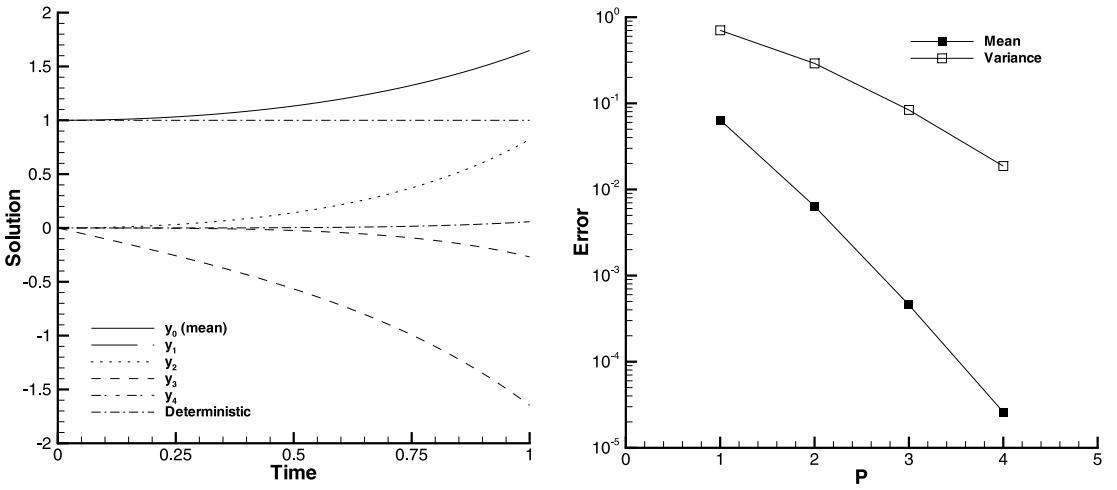

Fig. 2. Solution with Gaussian random input by fourth-order Hermite-chaos: left: solution of each random mode; right: error convergence of the mean and the variance.

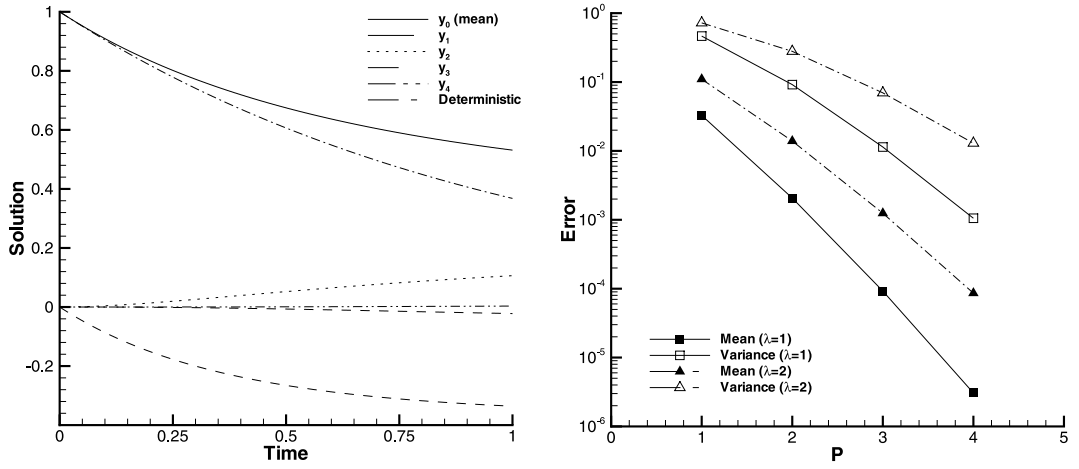

Fig. 3. Solution with Poisson random input by fourth-order Charlier-chaos: left: solution of each mode ($\lambda = 1$); right: error convergence of the mean and the variance with different λ.

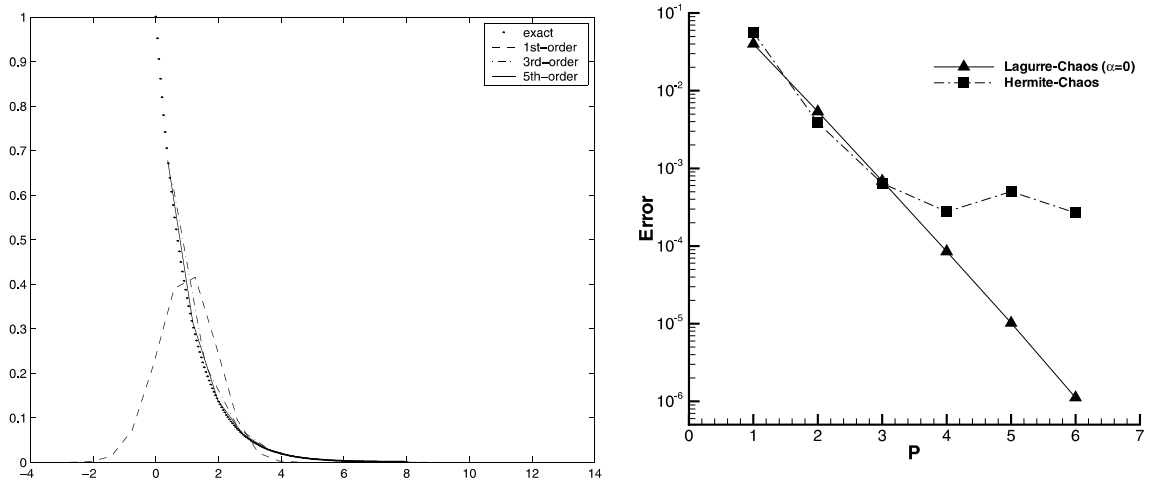

Fig. 4. Approximation of exponential distribution with Hermite-chaos: left: PDF of different orders of approximations of exponential random variable by Hermite-chaos; right: error convergence of the mean solution with Laguerre-chaos and Hermite-chaos.

we continue to use Hermite-chaos to solve the Eq. (46) with k being an exponential random variable, the exponential convergence rate will not be maintained as opposed to the Laguerre-chaos.

Another interesting example is shown in Fig. 5, when a beta random variable is approximated by the Hermite-chaos. The convergence of Hermite-chaos can be clearly seen from the approximated PDF compared with the exact PDF. The special case of $\alpha = \beta = 0$ corresponds to the uniform distribution, and we observe oscillations near the corners of the square. This is analogous to the familiar Gibb's phenomenon in the deterministic spectral approximation. In this case, the best choice is the Jacobi-chaos which can represent the beta random variable exactly with only the first-order term. We expect that exponential convergence rate will not be maintained if the non-optimal Hermite-chaos is used to solve Eq. (46) instead of the Jacobi-chaos.

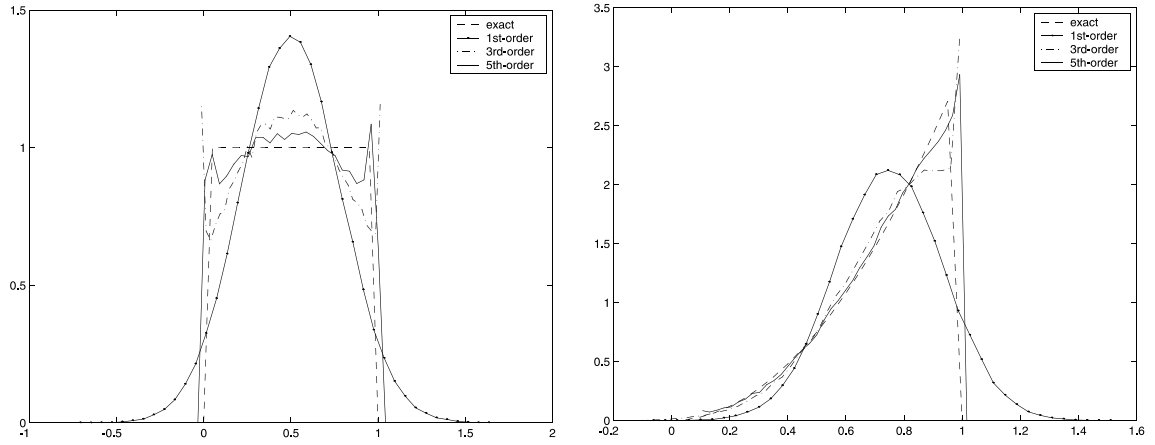

Fig. 5. PDF of approximations of Beta distributions by Hermite-chaos: left: $\alpha = \beta = 0$, the uniform distribution; right: $\alpha = 2$, $\beta = 0$.

5.2. Pressure-driven channel flow

We consider a pressure-driven channel flow as shown in Fig. 6, where the boundary conditions are considered to be uncertain. The domain (see Fig. 6) has dimensions such that $y \in [-1, 1]$ and $x \in [-5, 5]$. The pressure gradient, acting like a driving force, is equal to twice the kinematic viscosity, and thus for a no-slip wall condition the solution is a parabolic profile with centerline velocity equals unity.

5.2.1. Micro-channel flow: uniform boundary conditions

We assume that the boundary conditions at the two walls are uncertain with zero mean value, i.e., $u_1 = 0 + \sigma_1\xi_1$ and $u_2 = 0 + \sigma_2\xi_2$, where ξ_1 and ξ_2 are two independent random variables, and σ_1 and σ_2 are their corresponding standard deviations. Since the boundary conditions are uniform in space, with periodic boundary conditions specified in the streamwise direction, the nonlinear terms in the stochastic Navier–Stokes equations (33) vanish, and we obtain the exact solution

$$u(x,y) = (1-y^2) + \frac{1-y}{2}\sigma_1\xi_1 + \frac{1+y}{2}\sigma_2\xi_2, \quad v(x,y) = 0. \tag{53}$$

The solution consists of a parabolic profile for the mean solution and two linear random modes (ξ_1 and ξ_2) linearly distributed across the channel width. Note the form of the exact solution is independent of the distribution type of random variables ξ_1 and ξ_2.

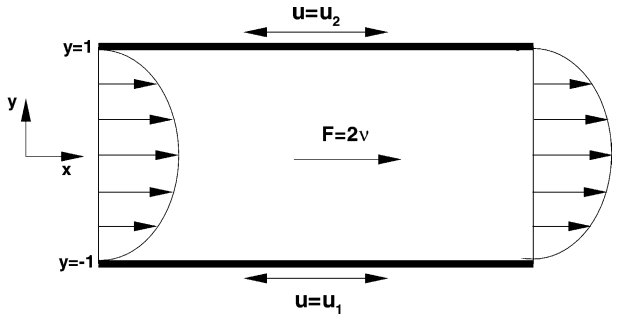

Fig. 6. Schematic of the domain for pressure-driven channel flow with random boundary conditions.

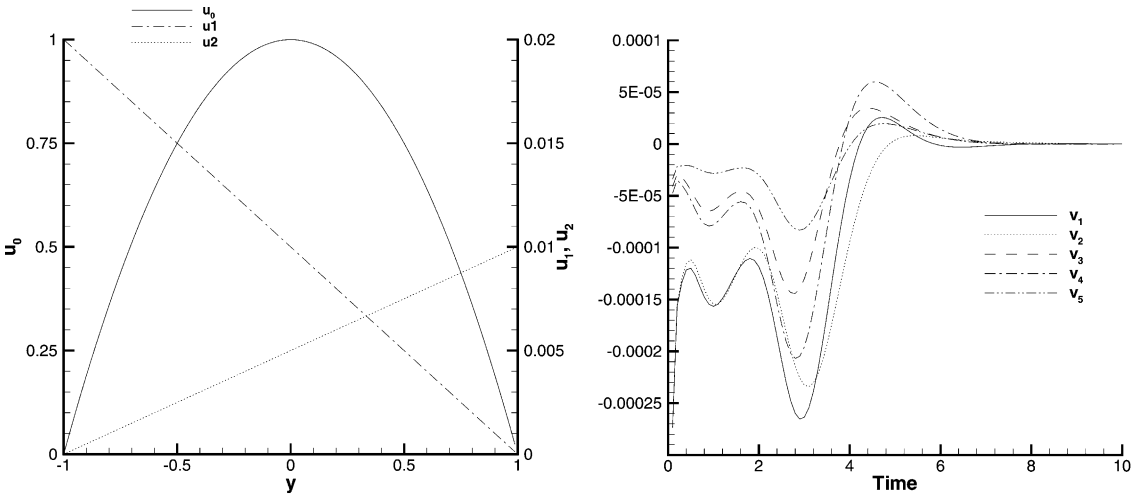

Fig. 7. Solution of the micro-channel with uniform Gaussian random boundary conditions: left: the solution profile; right: development of random modes of v-velocity with nonzero initial conditions.

On the left of Fig. 7 we show the solution profile across the channel. The ξ_1 and ξ_2 are two independent Gaussian random variables with $\sigma_1 = 0.02$ and $\sigma_2 = 0.01$. The two-dimensional ($n = 2$) Hermite-chaos, the optimal Askey-chaos in this case, is employed. Although the solution suggests that only a first-order expansion ($p = 1$) is needed, higher-order terms ($p > 1$) are included in the computation but are identically zero as expected. Another test is to set the initial condition of the flow to an arbitrary random state. We add perturbation terms to the exact solution (Eq. (53)) for each random mode in the form of $u_k(x, y, 0) = \alpha^p f(x, y)$ and $v_k(x, y, 0) = \alpha^p g(x, y)$ for $k = 0, \ldots, P$. Here p is the order of the chaos expansions and $0 < \alpha < 1$ to ensure the decaying of the perturbation. On the right of Fig. 7 we show the time history of some dominant random modes of v-velocity at the center of the channel. It is seen that due to the nonlinear interactions between the random modes some of them are amplified in the early stage, but eventually all modes converge to the exact solution.

Computations with other types of random inputs have been conducted with their corresponding Askey-chaos expansions. More specifically, we set ξ_1 and ξ_2 to be beta and gamma random variables and employ the Jacobi-chaos and Laguerre-chaos, respectively. Similar results were obtained with the results shown in Fig. 7.

5.2.2. Micro-channel flow: non-uniform boundary conditions

Next we consider the case of non-uniform random boundary conditions, i.e., the wall boundary conditions at different locations are partially correlated. The wall boundary conditions are assumed to be random processes with correlation function in the form

$$C(x_1, x_2) = \sigma^2 \mathrm{e}^{-(|x_1 - x_2|)/b}, \tag{54}$$

where b is the *correlation length*. This correlation function has been employed extensively to model processes in many fields; it is employed here because it allows us to solve the eigenvalue problem (24) of the Karhunen–Loeve expansion of Eq. (23) analytically. If this is not the case, a standard numerical eigenvalue solver can be used.

By setting a relatively large correlation length $b = 100$, the eigenvalues of the Karhunen–Loeve expansion are

$$\lambda_1 = 9.675354, \quad \lambda_2 = 0.1946362, \quad \lambda_3 = 0.05014117, \quad \ldots$$

Due to the fast decay of the eigenvalues, we use the first two terms in the Karhunen–Loeve expansion given by Eq. (23). This results in a two-dimensional chaos expansion ($n = 2$). Resolution-independence checks were conducted and the fourth-order chaos expansion ($p = 4$) were found to be sufficient to resolve the problem in the random space. Using Eq. (29) this results in a 15-term expansion ($P = 14$). Only the lower wall boundary condition is assumed to be uncertain with $\sigma = 0.1$, while the upper wall is stationary and deterministic. A parabolic velocity profile is specified at the inlet and zero Neumann condition at the outlet. A mesh with 10×2 elements is employed and basis Jacobi polynomials of sixth-order in each element results in resolution independent solution in space.

We first consider the lower wall boundary condition a Gaussian random process and employ the Hermite-chaos expansion. Fig. 8 shows the velocity contour plot of the deviation of the mean solution at steady-state from a parabolic profile. The mean of u-velocity remains close to the parabolic shape and the mean of v-velocity, although small in magnitude, is non-zero. Fig. 9 shows steady-state solutions of the

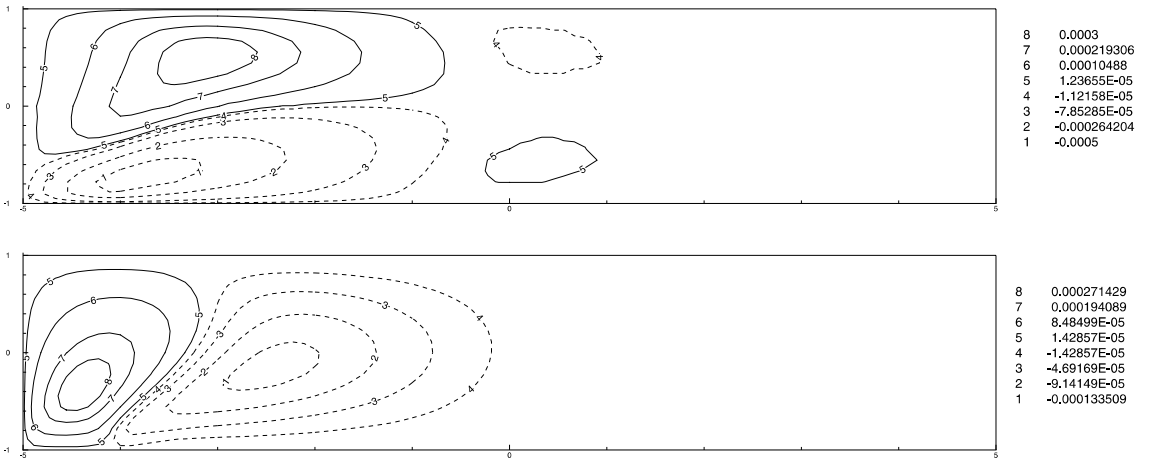

Fig. 8. Deviation of mean solution from a parabolic profile in micro-channel flow with partially correlated random boundary conditions at the lower wall: upper: u-velocity; lower: v-velocity.

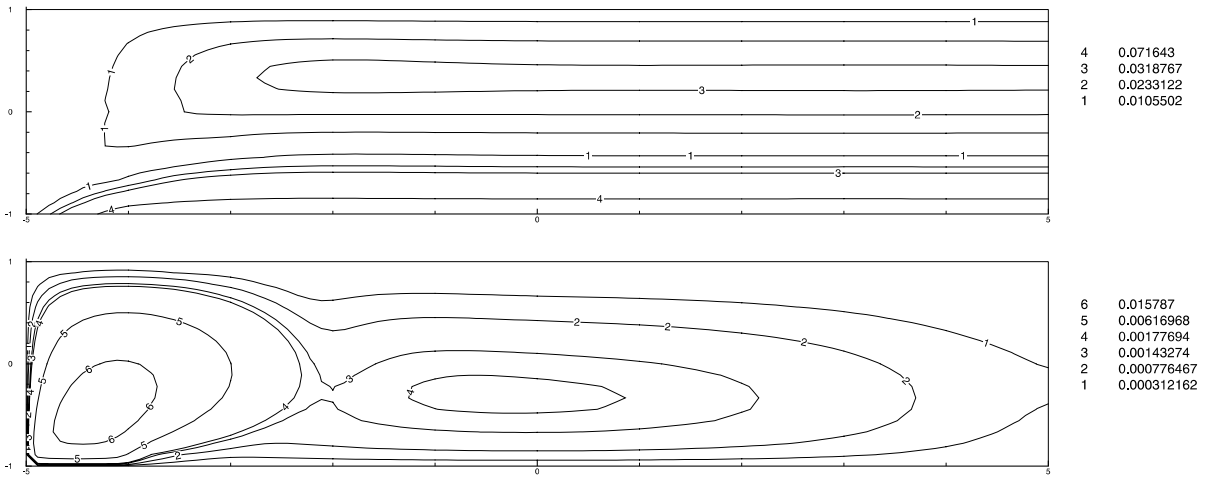

Fig. 9. Contours of *rms* of u-velocity (upper) and v-velocity (lower).

root-mean square (rms) of u and v-velocity. We see the development of a 'stochastic boundary layer' close to the lower wall. All the higher-order expansion terms are non-zero, which implies that although the random input is a Gaussian process, the solution output is *not* Gaussian. Since no analytic solution is available, Monte Carlo (MC) simulation is used to validate the result. Fig. 10 shows the solution of mean velocity u and v along the centerline of the channel. It is seen that the Monte Carlo solution converges non-monotonically to the Hermite-chaos result as the number of realizations increases. In this case, it is only after 40,000 realizations that Monte Carlo solution can capture the solution accurately, especially the nonlinear interactions close to the inlet. The polynomial chaos solver, with 15 terms in the expansions, is more than two thousands times faster than the Monte Carlo computation without using any special optimization techniques. In Fig. 11 the solution of the mean velocity along the centerline is shown corresponding to different values of σ. It can be seen that as the intensity of the input uncertainty σ increases the stochastic solution responses increase nonlinearly.

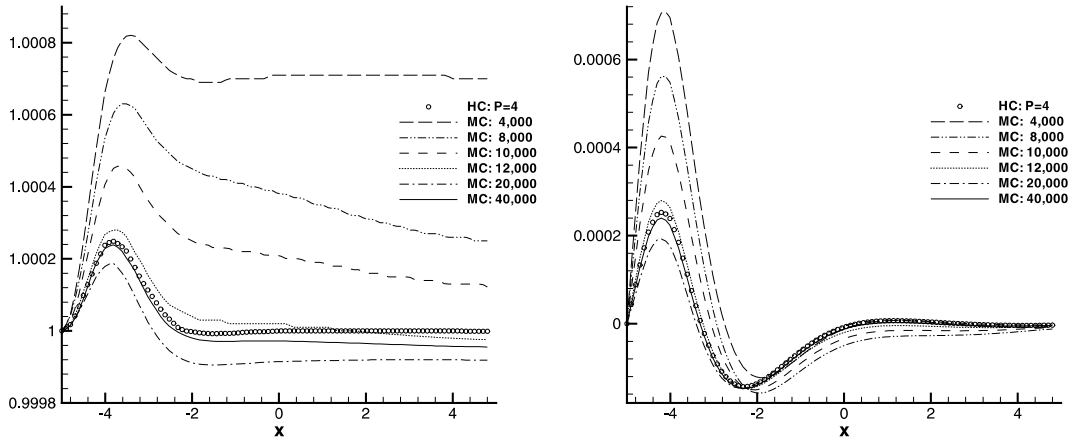

Fig. 10. Monte Carlo (MC) and Hermite-chaos (HC) solution of the mean velocities along the centerline of the channel: left: u-velocity; right: v-velocity.

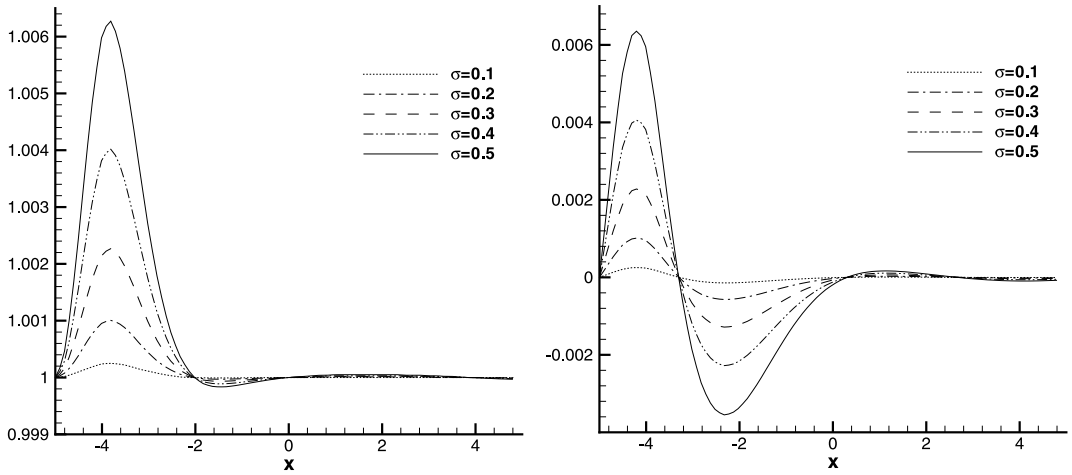

Fig. 11. Hermite-chaos solution of the mean velocities along the centerline of the channel with different σ: left: u-velocity; right: v-velocity.

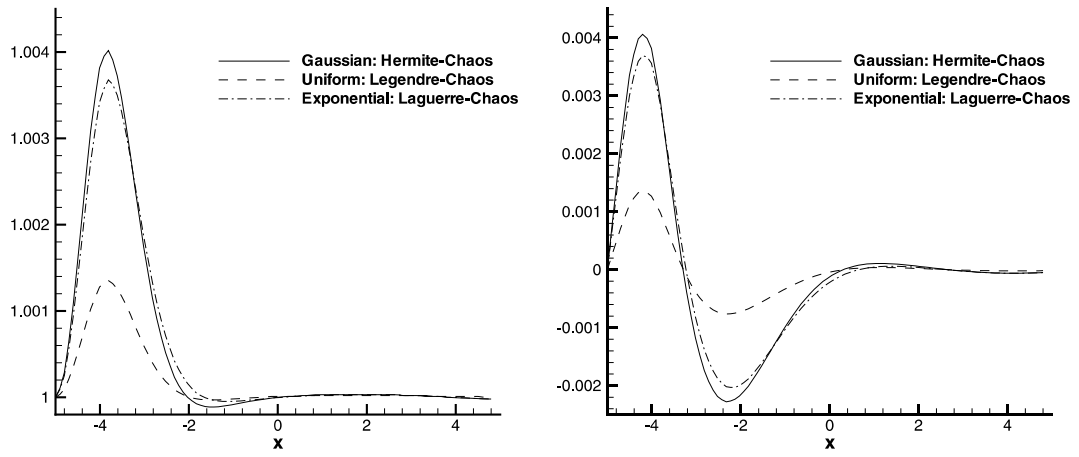

Fig. 12. Chaos solution of mean velocities along the centerline of the channel with different types of input processes: left: u-velocity; right: v-velocity.

In Fig. 12 we plot the mean solution along the centerline of the channel with different types of stochastic inputs. Specifically, we assume the random processes of the low wall boundary condition are zero-mean Gaussian, uniform and exponential processes with the same exponential correlation structure (Eq. (54)) and fixed parameter $\sigma = 0.4$. The corresponding Askey-chaos, i.e., the Hermite-, Legendre- and Laguerre-chaos, respectively, are employed. The variance of the velocity, non-dimensionalized by the input variance σ^2, is shown in Fig. 13. It is seen that the uniform random process results in a smoother solution with smaller variances due to the fact that the uniform distribution has finite support.

Fig. 14 shows the solution of mean velocity along the centerline of the channel corresponding to *uniform* stochastic process as the lower wall boundary conditions, with the same correlation structure as above

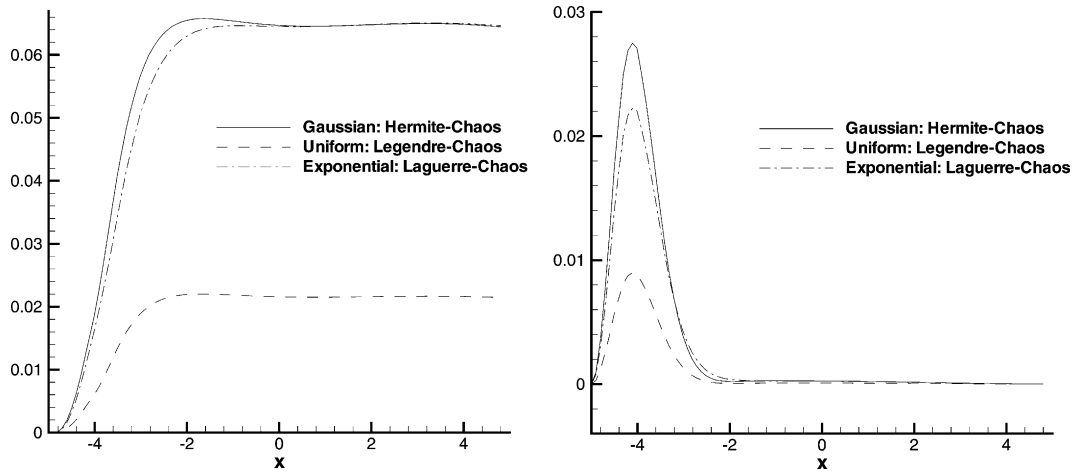

Fig. 13. Chaos solution of variance along the centerline of the channel with different types fo input processes: left: variance of u-velocity; right: variance of v-velocity.

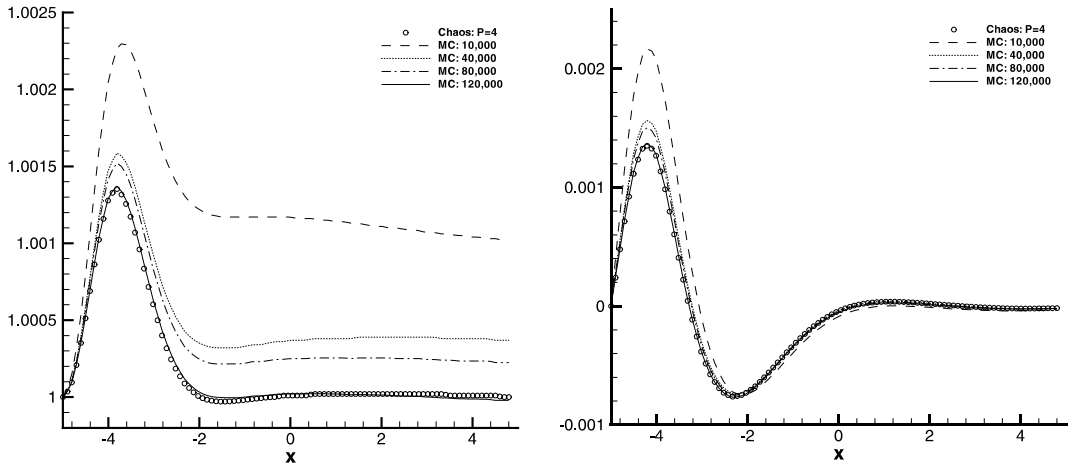

Fig. 14. Monte Carlo (MC) and Legendre-chaos solution of the mean velocities along the centerline of the channel with uniform stochastic inputs: left: u-velocity; right: v-velocity.

($\sigma = 0.4$). The Legendre-chaos expansion is employed. The Monte Carlo solution converges to the chaos solution; with 120,000 realizations it captures the nonlinear interactions near the inlet accurately. The Legendre-chaos corresponds to dimension $n = 2$ and polynomial order $p = 4$, which according to the formula of Eq. (29) gives 15 terms in the expansion.

5.3. Flow past a circular cylinder

In this section we simulate two-dimensional incompressible flow past a circular cylinder with random fluctuations superimposed to the freestream. More specifically, the inflow takes the form $u_{\text{in}} = \bar{u} + g$, where g is a random variable or process. Here we focus on the Gaussian process and Hermite-chaos solution. The size of the computational domain is $[-15, 25] \times [-9, 9]$ and the cylinder is at the origin $(0, 0)$ with diameter $D = 1$. The definition of Reynolds number is based on the mean value of the inflow velocity $\bar{u}$ and the diameter of the cylinder. The domain consists of 412 triangular elements with periodic conditions specified in the crossflow direction. Sixth-order Jacobi polynomial in each element is observed to result in resolution-independent solution in space for Reynolds number less than 200.

5.3.1. Flow close to first critical Reynolds number

It is well known that for two-dimensional flow past a circular cylinder, the first critical Reynolds number is around $Re \sim 40$, where the flow bifurcates from steady state to periodic vortex shedding [30]. Here we study the effects of the upstream random perturbations close to this Reynolds number. We set $u_{\text{in}} = \bar{u} + \sigma\xi$, where ξ is a Gaussian random variable and σ is its standard deviation. The one-dimensional Hermite-chaos expansion is thus employed. The pressure at the rear stagnation point of the cylinder is extremely sensitive to the vortex shedding state and is monitored in our computation.

Fig. 15 shows the time history of the mean pressure at the rear stagnation point at $Re = 40$, which is close to the critical Reynolds number. Solution with fourth-order and sixth-order Hermite-chaos are shown, together with the deterministic pressure history as reference. A negligible difference is observed between fourth-order and sixth-order chaos solutions (less than 0.1%). Thus, the solution can be considered as

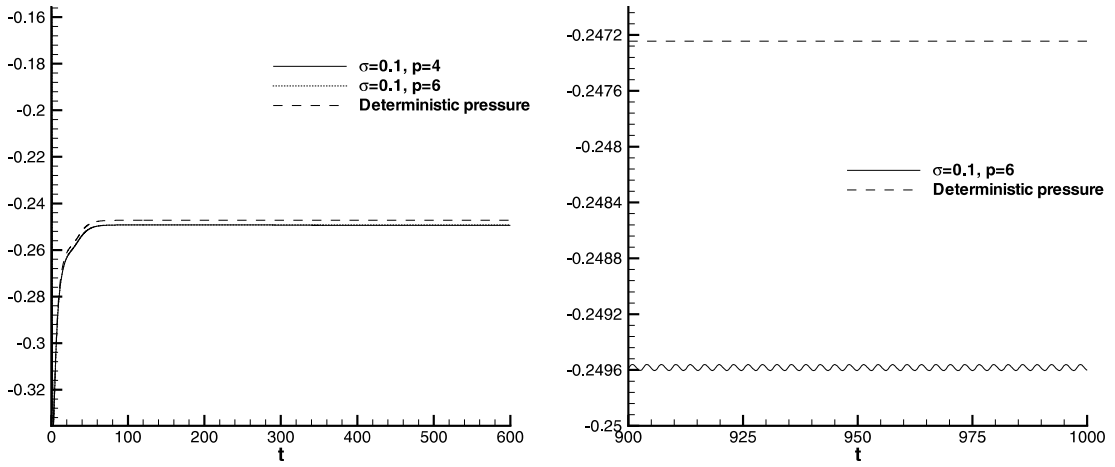

Fig. 15. Time history of mean pressure at the rear stagnation point at $Re = 40$ (Gaussian perturbation with $\sigma = 0.1$): left: the time history; right: close-up view.

resolution-independent in the random space. In the close-up view we see that the 10% random perturbation ($\sigma = 0.1$) triggers an instability and the flow becomes weakly periodic, as opposed to the deterministic solution which remains steady.

Next, we lower further the inflow Reynolds number to $Re = 35$. In Fig. 16 we show the time history of the mean pressure signal at the rear stagnation point. Again, resolution independence checks show a negligible difference (less than 0.1%) in the solutions by fourth-order and sixth-order Hermite-chaos. It is shown that at this Reynolds number a 10% random perturbation ($\sigma = 0.1$) is unable to trigger an instability and the flow remains steady. On the other hand, with a larger perturbation ($\sigma = 0.2$) the flow becomes weakly unsteady again.

These results suggest that the inflow random perturbations have noticeable effects on the stability of the flow near its critical Reynolds number. In fact, the existence of upstream perturbation induces the insta-

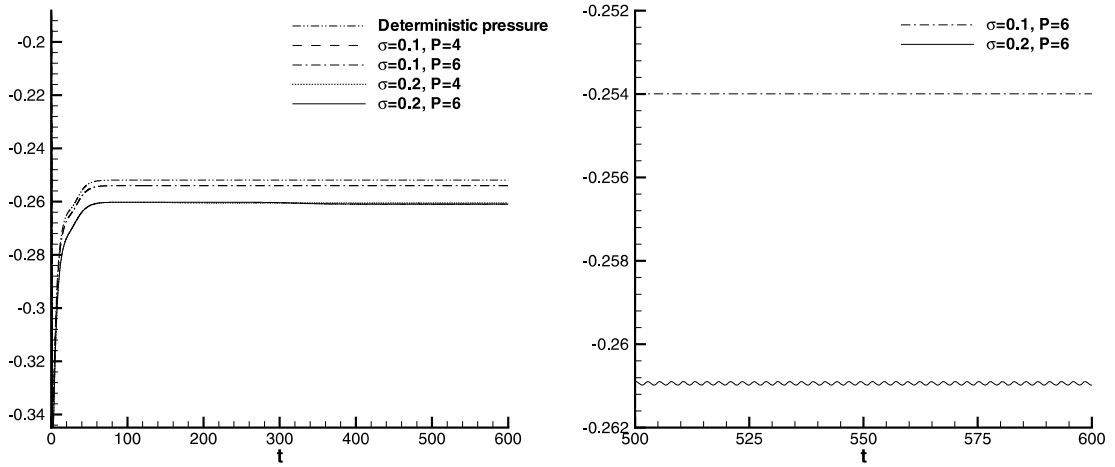

Fig. 16. Time history of mean pressure at the rear stagnation point at $Re = 35$: left: the time history; right: close-up view.

bility and forces the transition to occur at lower Reynolds number. This study is similar to that of Kaiktsis et al. [31] where the convective instability is studied by introducing random perturbations at the inflow of the backward-facing step flow. Instead of running many realizations of the deterministic flow solver, here we can resolve the propagation of inflow uncertainty by chaos expansion in one single run of the stochastic solver.

5.3.2. Flow at Re = 100

We consider another case at $Re = 100$ with freestream random velocity partially correlated. The inflow is $u_{\text{in}} = \bar{u} + g(y)$ where $g(y)$ is a Gaussian process with the exponential covariance kernel of Eq. (54) with $\sigma = 0.02$. Again, a relatively large correlation length is chosen ($b = 100$) so that the first two eigenmodes are adequate to represent the process by Karhunen–Loeve expansion (23). Thus, we employ a two-dimensional Hermite-chaos expansion ($n = 2$) and fourth-order chaos ($p = 4$).

Fig. 17 shows the pressure signal, together with the deterministic signal for reference (denoted as P_{D} in dotted line). We see that the stochastic *mean* pressure signal has a smaller amplitude and is out-of-phase with respect to the deterministic signal. Although initially, the stochastic response follows the deterministic response, eventually there is a change in the Strouhal frequency as shown in Fig. 18. Specifically, the Strouhal frequency of the mean stochastic solution is slightly lower than the deterministic one and has a broader support.

In Fig. 19 we present velocity profiles along the centerline for the deterministic and the mean stochastic solution at the same time instant. We see that significant quantitative differences emerge even with a relatively small 2% uncertainty in the freestream. In Fig. 20 we plot instantaneous vorticity contours for the mean of the vorticity and compared it with the corresponding plot from the deterministic simulation; we

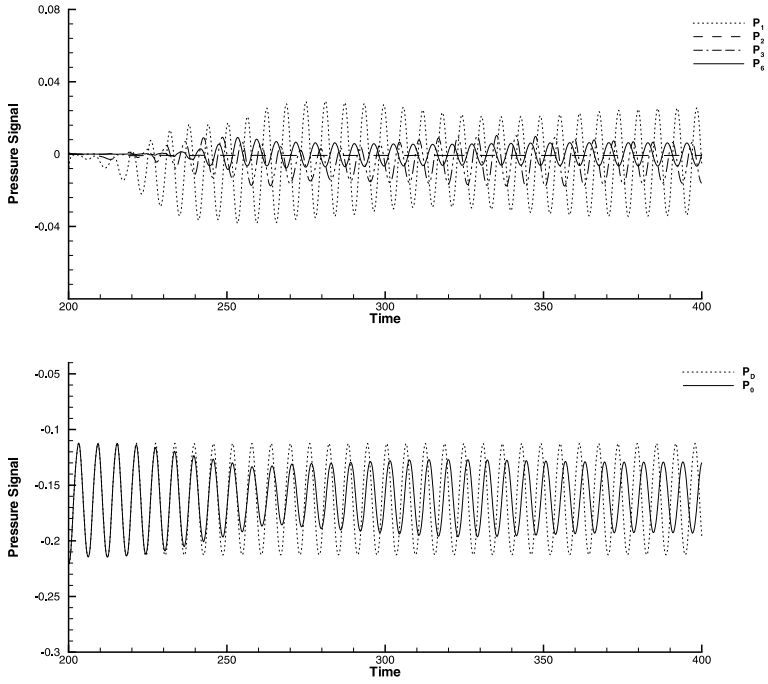

Fig. 17. Pressure signal of cylinder flow with non-uniform Gaussian random inflow: upper: high modes; lower: zero mode (mean).

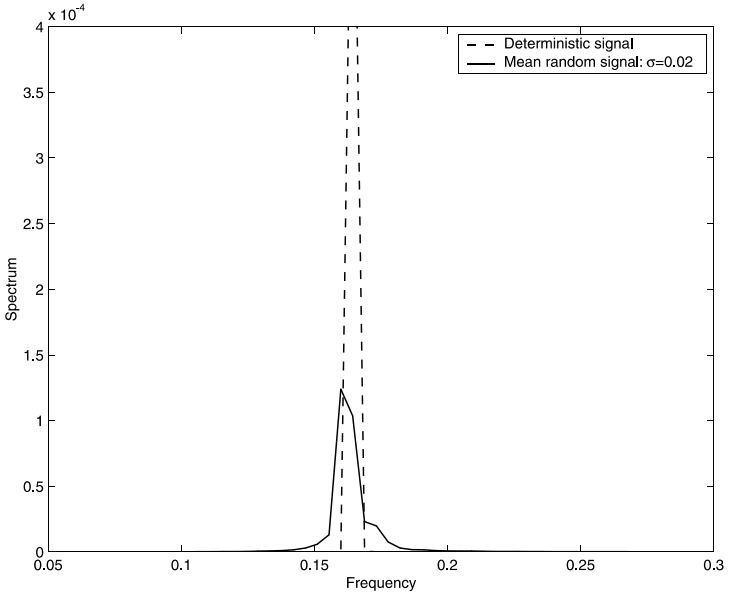

Fig. 18. Frequency spectrum for the deterministic (high peak) and stochastic simulation (low peak).

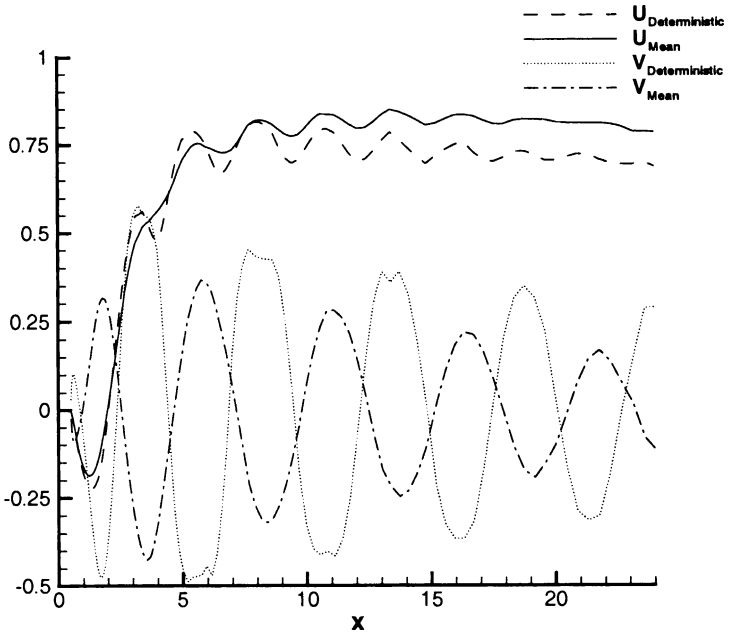

Fig. 19. Instantaneous profiles of the two velocity components along the centerline (in the wake) for the deterministic and the mean stochastic solution.

observe a diffusive effect induced by the randomness. In Fig. 21 we plot contours of the corresponding rms of vorticity. It shows that the uncertainty influences the most interesting region of the flow, i.e., the shear layers and the near-wake but not the far-field.

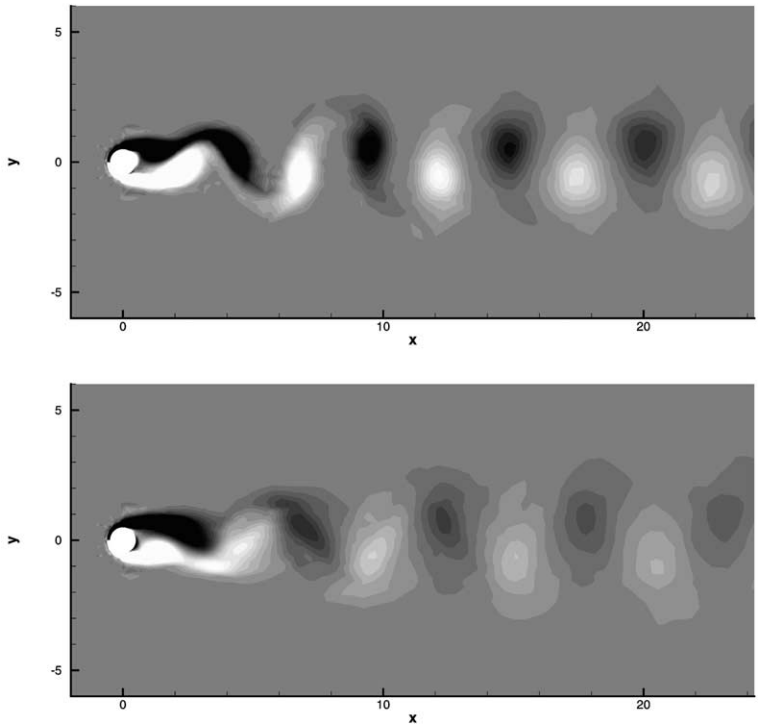

Fig. 20. Instantaneous vorticity field: upper: deterministic solution with uniform inflow; lower: mean solution with non-uniform Gaussian random inflow.

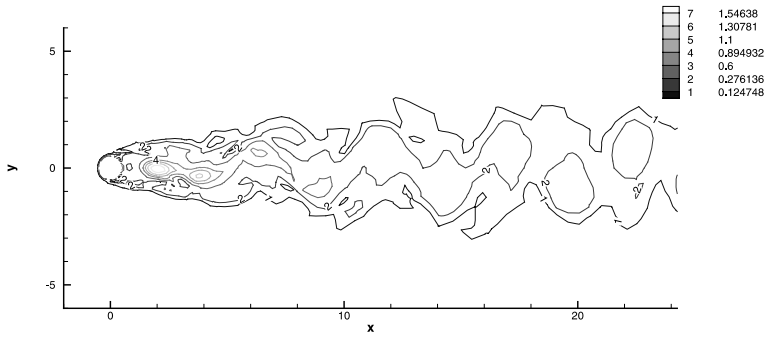

Fig. 21. Instantaneous contours of rms of vorticity field with non-uniform Gaussian random inflow.

6. Summary and discussion

We have developed a stochastic spectral method to model uncertainty and its propagation in simulations of incompressible flows. Numerical examples were presented for uncertain boundary conditions but the method can also be applied to model uncertainty in the boundary domain, e.g., a rough surface, in the transport coefficients, e.g., the eddy viscosity in large eddy simulations and other transport models, or in interaction forces for coupled problems. It provides a formal procedure for constructing a *composite error*

bar for CFD applications, as proposed in [32], that includes, in addition to the discretization errors, contributions due to imprecise physical inputs to the simulation.

More specifically, we have generalized the original polynomial chaos idea of Wiener and proposed a broader framework, i.e., the Askey-chaos, which includes Wiener's Hermite-chaos as a subset. For the most commonly known probability distributions, there exists a corresponding "best" orthogonal functional, in the sense that it leads to the substantial *dimensional reducibility*. We also applied the Askey-chaos expansion to the Navier–Stokes equations to model uncertainty in incompressible flow simulations for steady and unsteady problems. Convergence was verified with comparisons against exact solutions and solutions from Monte Carlo simulations for steady-state problems.

As regards efficiency, a single Askey-chaos based simulation, albeit computationally more expensive than the deterministic Navier–Stokes solver, is able to generate the solution statistics in a single run. Specifically, an Askey-chaos Navier–Stokes simulation with a total number of terms $(P+1)$ is approximately $(P+1)$ times more expensive than the corresponding deterministic one. (The overhead associated with the coupling terms is negligible.) In contrast, for the Monte Carlo simulation, tens of thousands of realizations are required for converged statistics, which is prohibitively expensive for most CFD problems in practice. For the problems we studied here we can only make direct comparisons for the steady-state cases, e.g., the micro-channel flow with random boundary conditions. In the case of the Hermite-chaos, the speed-up factor is approximately 2500 (see Fig. 10; (40,000/15)) for comparable accuracy of the first two moments. Similarly, for the Legendre-chaos the speed-up factor is about 8000 (see Fig. 14; (120,000/15)). Clearly, better Monte Carlo algorithms (e.g., accelerated versions with variance reduction) could reduce this factor but we still expect a three orders of magnitude speed-up for most problems involving a relatively low number of random dimensions.

There are, however, several open problems that need to be resolved for the Askey-chaos to be a robust and effective tool for modeling uncertainty. In particular, further research is required on:

- *Convergence rate*. The relatively poor resolution properties of Hermite and Laguerre expansions, compared to other spectral polynomials, are well documented in the literature [33,34]. However, re-scaling procedures, as done in [35], can be applied or a change of the trial basis from the Askey scheme, as demonstrated in Section 5.1.4, can be employed to accelerate convergence.
- *Dimensionality of the stochastic input*. This, in turn, determines the dimensionality of the random space and correspondingly the computational complexity of the problem. For a physical input random process with a very short correlation length, a high dimensional chaos expansion is required. As shown in Eq. (29), the number of expansion terms $(P+1)$ increases fast, although algebraically, both with the dimension n as well as the polynomial order p. In contrast, the convergence rate of the Monte Carlo method is independent of the number of random dimensions.
- *Interaction with spatial/temporal discretization.* In this paper, we have employed a multi-step time integrator and spectral/*hp* element methods for discretizing the deterministic operators. Some of the conclusions of the work presented here may not be readily extended to other discretizations.

The aforementioned issues can be addressed by systematic studies, investigating, for example, different type projections, filtering, proper trial basis, rescaling, etc. We are currently working in addressing some of these issues and we will report results in future publications.

Acknowledgements

We thank Mr. D. Lucor, Prof. C.-H. Su, and Prof. R. Ghanem for their useful suggestions. This work was supported by ONR and DOE. Computations were performed at Brown's TCASCV and NCSA's (University of Illinois) facilities.

Appendix A. Some orthogonal polynomials in Askey scheme

In this section we briefly review the definitions and properties of some important orthogonal polynomials from Askey scheme, which are discussed in this paper for the Wiener–Askey polynomial chaos.

A.1. Continuous polynomials

A.1.1. Hermite polynomial $H_n(x)$ and Gaussian distribution

Definition:

$$H_n(x) = (2x)^n {}_2F_0\left(-\frac{n}{2}, -\frac{n-1}{2}; \ ; -\frac{1}{x^2}\right). \tag{A.1}$$

Orthogonality:

$$\frac{1}{\sqrt{\pi}} \int_{-\infty}^{\infty} \mathrm{e}^{-x^2} H_m(x) H_n(x)\,\mathrm{d}x = 2^n n! \delta_{mn}. \tag{A.2}$$

Recurrence relation:

$$H_{n+1}(x) - 2xH_n(x) + 2nH_{n-1}(x) = 0. \tag{A.3}$$

Rodriguez formula:

$$\mathrm{e}^{-x^2} H_n(x) = (-1)^n \frac{d^n}{dx^n}\left(\mathrm{e}^{-x^2}\right). \tag{A.4}$$

The weighting function is $w(x) = \mathrm{e}^{-x^2}$ from the orthogonality condition (A.2). After rescaling x by $\sqrt{2}$, the weighting function is the same as the probability density function of a standard *Gaussian* random variable with zero mean and unit variance.

A.1.2. Laguerre polynomial $L_n^{(\alpha)}(x)$ and Gamma distribution

Definition:

$$L_n^{(\alpha)}(x) = \frac{(\alpha+1)_n}{n!} \, {}_1F_1(-n; \alpha+1; x). \tag{A.5}$$

Orthogonality:

$$\int_0^{\infty} \mathrm{e}^{-x} x^{\alpha} L_m^{(\alpha)}(x) L_n^{(\alpha)}(x)\,\mathrm{d}x = \frac{\Gamma(n+\alpha+1)}{n!}\delta_{mn}, \quad \alpha > -1. \tag{A.6}$$

Recurrence relation:

$$(n+1)L_{n+1}^{(\alpha)}(x) - (2n+\alpha+1-x)L_n^{(\alpha)}(x) + (n+\alpha)L_{n-1}^{(\alpha)}(x) = 0. \tag{A.7}$$

Rodriguez formula:

$$\mathrm{e}^{-x} x^{\alpha} L_n^{(\alpha)}(x) = \frac{1}{n!}\frac{\mathrm{d}^n}{\mathrm{d}x^n}(\mathrm{e}^{-x} x^{n+\alpha}). \tag{A.8}$$

Recall that the Gamma distribution has the probability density function

$$f(x) = \frac{x^{\alpha}\mathrm{e}^{-x/\beta}}{\beta^{\alpha+1}\Gamma(\alpha+1)}, \quad \alpha > -1, \ \ \beta > 0. \tag{A.9}$$

Despite of the scale parameter β and a constant factor $\Gamma(\alpha+1)$, it is the same as the weighting function of Laguerre polynomial.

A.1.3. Jacobi polynomial $P_n^{(\alpha,\beta)}(x)$ and Beta distribution

Definition:

$$P_n^{(\alpha,\beta)}(x) = \frac{(\alpha+1)_n}{n!}\,{}_2F_1\left(-n, n+\alpha+\beta+1; \alpha+1; \frac{1-x}{2}\right). \tag{A.10}$$

Orthogonality:

$$\int_{-1}^{1}(1-x)^{\alpha}(1+x)^{\beta}P_m^{(\alpha,\beta)}(x)P_n^{(\alpha,\beta)}(x)\,\mathrm{d}x = h_n^2\delta_{mn}, \quad \alpha > -1, \ \ \beta > -1, \tag{A.11}$$

where

$$h_n^2 = \frac{2^{\alpha+\beta+1}}{2n+\alpha+\beta+1}\,\frac{\Gamma(n+\alpha+1)\Gamma(n+\beta+1)}{\Gamma(n+\alpha+\beta+1)n!}.$$

Recurrence relation:

$$\begin{aligned} xP_n^{(\alpha,\beta)}(x) = {} & \frac{2(n+1)(n+\alpha+\beta+1)}{(2n+\alpha+\beta+1)(2n+\alpha+\beta+2)}P_{n+1}^{(\alpha,\beta)}(x) + \frac{\beta^2-\alpha^2}{(2n+\alpha+\beta)(2n+\alpha+\beta+2)}P_n^{(\alpha,\beta)}(x) \\ & + \frac{2(n+\alpha)(n+\beta)}{(2n+\alpha+\beta)(2n+\alpha+\beta+1)}P_{n-1}^{(\alpha,\beta)}(x). \end{aligned} \tag{A.12}$$

Rodriguez formula:

$$(1-x)^{\alpha}(1+x)^{\beta}P_n^{(\alpha,\beta)}(x) = \frac{(-1)^n}{2^n n!}\,\frac{\mathrm{d}^n}{\mathrm{d}x^n}[(1-x)^{n+\alpha}(1+x)^{n+\beta}]. \tag{A.13}$$

The Beta distribution has the probability density function

$$f(x) = \frac{(x-a)^{\beta}(b-x)^{\alpha}}{(b-a)^{\alpha+\beta+1}B(\alpha+1,\beta+1)}, \quad a \leqslant x \leqslant b, \tag{A.14}$$

where $B(p,q)$ is the *Beta function* defined as

$$B(p,q) = \frac{\Gamma(p)\Gamma(q)}{\Gamma(p+q)}. \tag{A.15}$$

It is clear that despite of a constant factor the weighting function of Jacobi polynomial $w(x) = (1-x)^{\alpha}(1+x)^{\beta}$ from (A.11) is the same as the probability density function of Beta distribution defined in domain $[-1,1]$. When $\alpha = \beta = 0$, the Jacobi polynomials become the Legendre polynomials and the weighting function is a constant which corresponds to the important *uniform distribution*.

A.2. Discrete polynomials

A.2.1. Charlier polynomial $C_n(x;a)$ and Poisson distribution

Definition:

$$C_n(x;a) = {}_2F_0\left(-n, -x; \ ; -\frac{1}{a}\right). \tag{A.16}$$

Orthogonality:

$$\sum_{x=0}^{\infty} \frac{a^x}{x!} C_m(x;a) C_n(x;a) = a^{-n} \mathrm{e}^a n! \delta_{mn}, \quad a > 0. \tag{A.17}$$

Recurrence relation:

$$-xC_n(x;a) = aC_{n+1}(x;a) - (n+a)C_n(x;a) + nC_{n-1}(x;a). \tag{A.18}$$

Rodriguez formula:

$$\frac{a^x}{x!} C_n(x;a) = \nabla^n \left(\frac{a^x}{x!} \right), \tag{A.19}$$

where ∇ is the backward difference operator defined as

$$\Delta f(x) = f(x+1) - f(x) \quad \text{and} \quad \nabla f(x) = f(x) - f(x-1). \tag{A.20}$$

The probability function of *Poisson* distribution is

$$f(x;a) = \mathrm{e}^{-a} \frac{a^x}{x!}, \quad k = 0, 1, 2, \ldots. \tag{A.21}$$

Despite of a constant factor e^{-a}, it is the same as the weighting function of Charlier polynomials.

A.2.2. Krawtchouk polynomial $K_n(x;p,N)$ and binomial distribution

Definition:

$$K_n(x;p,N) = {}_2F_1\left(-n, -x; -N; \frac{1}{p} \right), \quad n = 0, 1, \ldots, N. \tag{A.22}$$

Orthogonality:

$$\sum_{x=0}^{N} \binom{N}{x} p^x (1-p)^{N-x} K_m(x;p,N) K_n(x;p,N) = \frac{(-1)^n n!}{(-N)_n} \left(\frac{1-p}{p} \right)^n \delta_{mn}, \quad 0 < p < 1. \tag{A.23}$$

Recurrence relation:

$$-xK(x;p,N) = p(N-n)K_{n+1}(x;p,N) - [p(N-n) + n(1-p)]K_n(x;p,N) + n(1-p)K_{n-1}(x;p,N). \tag{A.24}$$

Rodriguez formula:

$$\binom{N}{x} \left(\frac{p}{1-p} \right)^x K_n(x;p,N) = \nabla^n \left[\binom{N-n}{x} \left(\frac{p}{1-p} \right)^x \right]. \tag{A.25}$$

Clearly, the weighting function from (A.23) is the probability function of the *binomial* distribution.

A.2.3. Meixner polynomial $M_n(x;\beta,c)$ and negative binomial distribution

Definition:

$$M_n(x;\beta,c) = {}_2F_1\left(-n, -x; \beta; 1 - \frac{1}{c} \right). \tag{A.26}$$

Orthogonality:

$$\sum_{x=0}^{\infty} \frac{(\beta)_x}{x!} c^x M_m(x;\beta,c) M_n(x;\beta,c) = \frac{c^{-n} n!}{(\beta)_n (1-c)^{\beta}} \delta_{mn}, \quad \beta > 0, \ \ 0 < c < 1. \tag{A.27}$$

Recurrence relation:

$$(c-1)x M_n(x;\beta,c) = c(n+\beta) M_{n+1}(x;\beta,c) - [n + (n+\beta)c] M_n(x;\beta,c) + n M_{n-1}(x;\beta,c). \tag{A.28}$$

Rodriguez formula:

$$\frac{(\beta)_x c^x}{x!} M_n(x;\beta,c) = \nabla^n \left[\frac{(\beta+n)_x c^x}{x!} \right]. \tag{A.29}$$

The weighting function is

$$f(x) = \frac{(\beta)_x}{x!} (1-c)^{\beta} c^x, \quad 0 < p < 1, \ \ \beta > 0, \ \ x = 0, 1, 2, \ldots. \tag{A.30}$$

It can verified that it is the probability function of *negative binomial* distribution. In the case of β being integer, it is often called the *Pascal* distribution.

A.2.4. Hahn polynomial $Q_n(x;\alpha,\beta,N)$ and hypergeometric distribution

Definition:

$$Q_n(x;\alpha,\beta,N) = {}_3F_2(-n, n+\alpha+\beta+1, -x; \alpha+1, -N; 1), \quad n = 0, 1, \ldots, N. \tag{A.31}$$

Orthogonality: For $\alpha > -1$ and $\beta > -1$ or for $\alpha < -N$ and $\beta < -N$,

$$\sum_{x=0}^{N} \binom{a+x}{x} \binom{\beta+N-x}{N-x} Q_m(x;\alpha,\beta,N) Q_n(x;\alpha,\beta,N) = h_n^2 \delta_{mn}, \tag{A.32}$$

where

$$h_n^2 = \frac{(-1)^n (n+\alpha+\beta+1)_{N+1} (\beta+1)_n n!}{(2n+\alpha+\beta+1)(\alpha+1)_n (-N)_n N!}.$$

Recurrence relation:

$$-x Q_n(x) = A_n Q_{n+1}(x) - (A_n + C_n) Q_n(x) + C_n Q_{n-1}(x), \tag{A.33}$$

where

$$Q_n(x) := Q_n(x;\alpha,\beta,N)$$

and

$$A_n = \frac{(n+\alpha+\beta+1)(n+\alpha+1)(N-n)}{(2n+\alpha+\beta+1)(2n+\alpha+\beta+2)},$$

$$C_n = \frac{n(n+\alpha+\beta+N+1)(n+\beta)}{(2n+\alpha+\beta)(2n+\alpha+\beta+1)}.$$

Rodriguez formula:

$$w(x;\alpha,\beta,N)Q_n(x;\alpha,\beta,N) = \frac{(-1)^n(\beta+1)_n}{(-N)_n}\nabla^n[w(x;\alpha+n,\beta+n,N-n)], \tag{A.34}$$

where

$$w(x;\alpha,\beta,N) = \binom{\alpha+x}{x}\binom{\beta+N-x}{N-x}.$$

If we set $\alpha = -\tilde{\alpha}-1$ and $\beta = -\tilde{\beta}-1$, we obtain

$$\tilde{w}(x) = \left[1\Big/\binom{N-\tilde{\alpha}-\tilde{\beta}-1}{N}\right]\left[\binom{\tilde{\alpha}}{x}\binom{\tilde{\beta}}{N-x}\Big/\binom{\tilde{\alpha}+\tilde{\beta}}{N}\right].$$

Apart from the constant factor $1/\binom{N-\tilde{\alpha}-\tilde{\beta}-1}{N}$, this is the definition of *hypergeometric* distribution.

References

[1] Workshop on Validation and Verification of Computational Mechanics Codes, Technical Report, Caltech, December, 1998.
[2] Workshop on Predictability of Complex Phenomena, Los Alamos, 6–8 December 1999, Technical Report.
[3] Workshop on Decision Making Under Uncertainty, IMA, 16–17 September 1999, Technical Report.
[4] T.J. Oden, W. Wu, M. Ainsworth, An a posteriori error estimate for finite element approximations of the Navier–Stokes equations, Comput. Meth. Appl. Mech. Eng. 111 (1994) 185.
[5] L. Machiels, J. Peraire, A.T. Patera, A posteriori finite element output bounds for the incompressible Navier–Stokes equations; application to a natural convection problem, J. Comput. Phys. 172 (2001) 401–425.
[6] R.G. Hills and T.G. Trucano, Statistical validation of engineering and scientific models: background, Technical Report SAND99-1256, Sandia National Laboratories, 1999.
[7] M. Shinozuka and G. Deodatis, Response variability of stochastic finite element systems, Technical Report, Department of Civil Engineering, Columbia University, New York, 1986.
[8] R.G. Ghanem, P. Spanos, Stochastic Finite Elements: A Spectral Approach, Springer, Berlin, 1991.
[9] N. Wiener, The homogeneous chaos, Am. J. Math. 60 (1938) 897–936.
[10] N. Wiener, Nonlinear Problems in Random Theory, MIT Technology Press and John Wiley and Sons, New York, 1958.
[11] W.C. Meecham, A. Siegel, Wiener–Hermite expansion in model turbulence at large Reynolds numbers, Phys. Fluids 7 (1964) 1178–1190.
[12] A. Siegel, T. Imamura, W.C. Meecham, Wiener–Hermite expansion in model turbulence in the late decay stage, J. Math. Phys. 6 (1965) 707–721.
[13] W.C. Meecham, D.T. Jeng, Use of the Wiener–Hermite expansion for nearly normal turbulence, J. Fluid Mech. 32 (1968) 225–249.
[14] S.A. Orszag, L.R. Bissonnette, Dynamical properties of truncated Wiener–Hermite expansions, Phys. Fluids 10 (1967) 2603.
[15] S.C. Crow, G.H. Canavan, Relationship between a Wiener–Hermite expansion and an energy cascade, J. Fluid Mech. 41 (1970) 387–403.
[16] A.J. Chorin, Gaussian fields and random flow, J. Fluid Mech. 85 (1974) 325–347.
[17] R. Askey, J. Wilson, Some basic hypergeometric polynomials that generalize Jacobi polynomials, Memoirs of the American Mathematical Society, AMS, Providence, RI, 1985, p. 319.
[18] G. Szegö, Orthogonal Polynomials, AMS, Providence, RI, 1939.
[19] P. Beckmann, Orthogonal Polynomials for Engineers and Physicists, Golem Press, 1973.
[20] T.S. Chihara, An Introduction to Orthogonal Polynomials, Gordon and Breach Science Publishers, 1978.
[21] R. Koekoek and R.F. Swarttouw. The Askey-scheme of hypergeometric orthogonal polynomials and its q-analogue, Technical Report 98-17, Department of Technical Mathematics and Informatics, Delft University of Technology, 1998.
[22] W. Schoutens, Stochastic Processes and Orthogonal Polynomials, Springer, New York, 2000.
[23] R.H. Cameron, W.T. Martin, The orthogonal development of nonlinear functionals in series of Fourier– Hermite functionals, Ann. Math. 48 (1947) 385.
[24] R.G. Ghanem, Stochastic finite elements for heterogeneous media with multiple random non-Gaussian properties, ASCE J. Eng. Mech. 125 (1) (1999) 26–40.

[25] R.G. Ghanem, Ingredients for a general purpose stochastic finite element formulation, Comput. Meth. Appl. Mech. Eng. 168 (1999) 19–34.
[26] H. Ogura, Orthogonal functionals of the Poisson process, IEEE Trans. Info. Theory 18 (1972) 473–481.
[27] M. Loéve, Probability Theory, fourth ed., Springer-Verlag, Berlin, 1977.
[28] G.E. Karniadakis, M. Israeli, S.A. Orszag, High-order splitting methods for incompressible Navier–Stokes equations, J. Comput. Phys. 97 (1991) 414.
[29] G.E. Karniadakis, S.J. Sherwin, Spectral/hp Element Methods for CFD, Oxford University Press, Oxford, 1999.
[30] C.H.K. Williamson, Vortex dynamics in the cylinder wake, Annu. Rev. Fluid Mech. 28 (1996) 477–539.
[31] L. Kaiktsis, G.E. Karniadakis, S.A. Orszag, Unsteadiness and convective instabilities in two-dimensional flow over a backward-facing step, J. Fluid Mech. 321 (1996) 157–187.
[32] G.E. Karniadakis, Towards an error bar in CFD, J. Fluids Eng. 117 (March) (1995).
[33] D. Gottlieb, S.A. Orszag, Numerical Analysis of Spectral Methods: Theory and Applications, CBMS-NSF, SIAM, Philadelphia, PA, 1977.
[34] J.P. Boyd, The rate of convergence of Hermite function series, Math. Comput. 35 (1980) 1039–1316.
[35] T. Tang, The Hermite spectral methods for Gaussian-type functions, SIAM J. Sci. Comput. 14 (1993) 594–606.